Contents

1. Introduction

This chapter presents the background of Öhlins, general suspension technologies and thorough description of their product. Chapter 1 also consists of the problem description in this thesis with accompanying purpose, aim and delimitations.

1.1. Background

1.1.1. Öhlins Racing AB

Öhlins Racing was founded in Sweden 1976 by Kenth Öhlin. For many years, the company has provided the racing, automotive and motorcycle industry with world class technology of suspension systems. Öhlins Racing extended their business area in the 1980's by developing pilot controlled pressure regulating hydraulic valves using electromagnetic actuators. The valves are an essential product to enable a suspension technology known as semi-active suspensions. This technology enables real time adjustments of the suspension damping characteristics and is mainly coveted within the automotive industry. Since November 2018, Öhlins Racing AB is a subsidiary of Tenneco Inc. Tenneco is one of the world's leading companies of ride performance and clean air technology.

1.1.2. Suspension Technologies

Suspension systems have been categorized into three major groups, passive, semi-active and fully active suspensions. The automotive industry demands tough requirements of the suspension system, regardless of the group. It is a tough market and it is a competition between different techonologies and between different companies. Passive, semi-active and fully active have each its advantages and disadvantages and a few are mentioned in their represented heading below. The characteristics of the suspension system are commonly discussed and are defined by velocity-force parameters, see Figure 1.1. The velocity-force diagram displays the capacity of each suspension technology. The velocity defines the direction and the velocity of the piston. In the velocity-force diagram, a negative force and velocity is referring to the rebound of the suspension. Also, a positive force and velocity is referred to the compression of the suspension. The size of the force determines the damping characteristics. A higher force yields a stiffer damping characteristic and a lower force yield a softer damping characteristics.

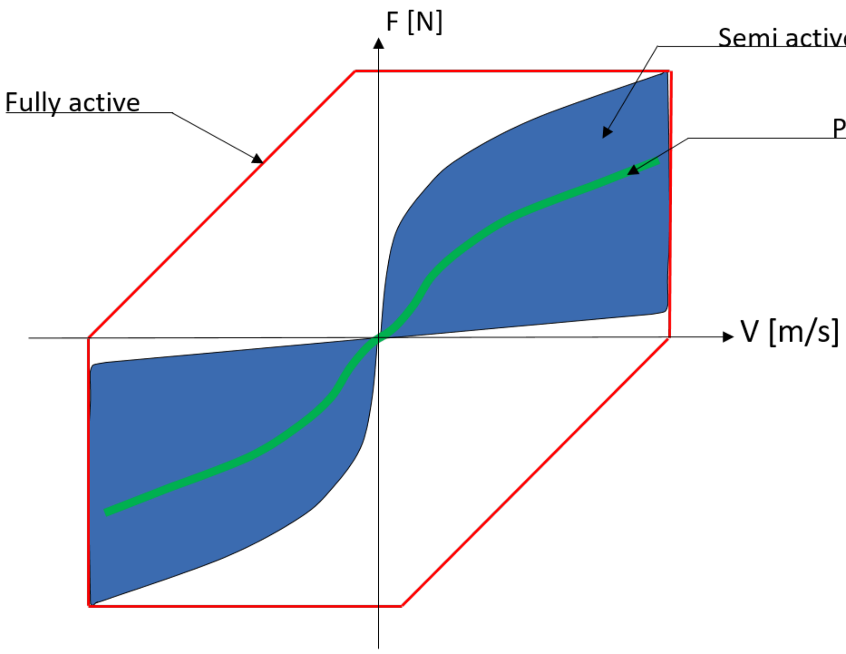

Figure 1.1.: Simplified visualization of the capacity of modern suspension technologies in a Force-Velocity diagram.

Passive suspension technology:
This technology has been on the market for the longest of the three. Passive suspensions are the cheapest to implement as it solely consists of a shock absorber. The system has lost market shares as the development of semi active and fully active systems has increased. This is due to the system is unable to change the characteristics of the damper as the damping coefficient is pre-set and manual adjustment is required, if possible.

Semi-active suspension technology:
Öhlins development of pressure regulating valves began with a patent in 1984. CES is the brand of Öhlins valves which enables semi-active suspensions and it stands for Continuously controlled Electronic Suspension. The system consists of a shock absorber, hydraulic valve, electromagnetic actuator, sensors and a control module. Unlike the passive suspension technology, the semi-active system alters the hydraulic flow within the shock-absorber. The adjustments of the hydraulic flow generate different internal pressures within the shock absorber. Different pressures yield different characteristics of the suspension system and the adjustments are performed without manual impositions of hands. The result of this is a suspension technology with both great handling and comfort characteristics with neither compromised.

Fully active suspension technology:
Unlike previous technologies, the fully active suspension technology can generate an independent force within the system to achieve great riding characteristics. To generate a force at high speed in curves, a lot of energy within the system is required.

1.1.3. Triple Tube Shock Absorber

A triple tube shock absorber enables a uniform hydraulic flow regardless of the shock absorber is being compressed or rebounded. Compression and rebound refers to the movement of the piston. A compressed shock absorber refers to an inward motion of the piston within the hydraulic cylinder. Rebound is referring to the opposite, when the piston moves outwards, see Figure 1.2. The function of a triple tube shock absorber is enabled by blow off and check valves within the piston and at the base of the damper. Öhlins external valve is used with the triple tube damper. An external valve refers to a valve which is externally mounted on the shock absorber.

Compression

During compression, the check valve is opened within the piston and closed at the base. This forces the fluid to flow through the piston. The blow off valve at the base prevents the pressure levels being too high within the compression chamber.

Rebound

During rebound, the check valve is closed within the piston and prevents the fluid to pass through the piston. The fluid is then forced to flow upwards according to the arrows in Figure 1.2. The blow off valve within the piston prevents the pressure levels being too high within the rebound chamber.

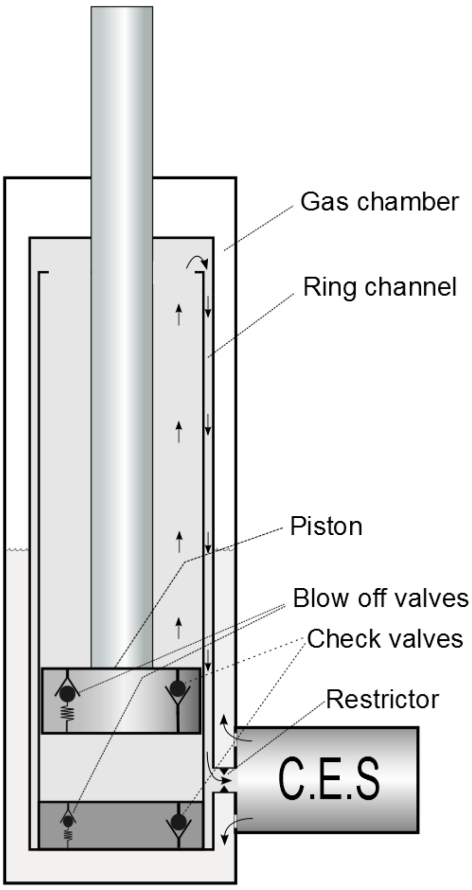

Figure 1.2.: Triple tube damper assembled with CES valve

1.1.4. Main Stage and Pilot Stage

The CES valve is a pilot controlled pressure regulating hydraulic valve using an electromagnetic actuator. Pressure regulation within the valve sets the pressure within the damper with real time adjustments using a force generated by a solenoid. The solenoid consists of a coil and a plunger which, using electrical current generates an axial force. Pressure is built up within the valve by throttling the hydraulic flow. The usage of a triple tube shock absorber together with an external CES valve results in an uniform hydraulic flow regardless of the stroke direction. There are two possible flows within the hydraulic valve, defined as main stage and pilot stage. The majority flows through the main stage but the pilot flow is required to enable pressure regulating characteristics.

The pilot stage acts as a trigger to control the main stage. The pilot stage controls the pressure at (B) by differentiating the generated force of the solenoid, displayed as F. The main stage is relieved as the main poppet orifice is opened, which occurs when the pressure P1 is in equilibrium with the main spring and the pressure located at B. The pressure at (B) is a result of a closed main poppet orifice. As the pressure within the system increases, the pilot poppet orifice is opened as the pressure at (B) together with the pilot poppet spring generates a force that is equal in size compared to the force generated by the solenoid and the system pressure P2. As the pilot poppet orifice is opened, the pressure at (B) is relieved through the escape passage. The resulting pressure drop at the main poppet opens the main poppet orifice and relieves the main stage, see Figure 1.3.

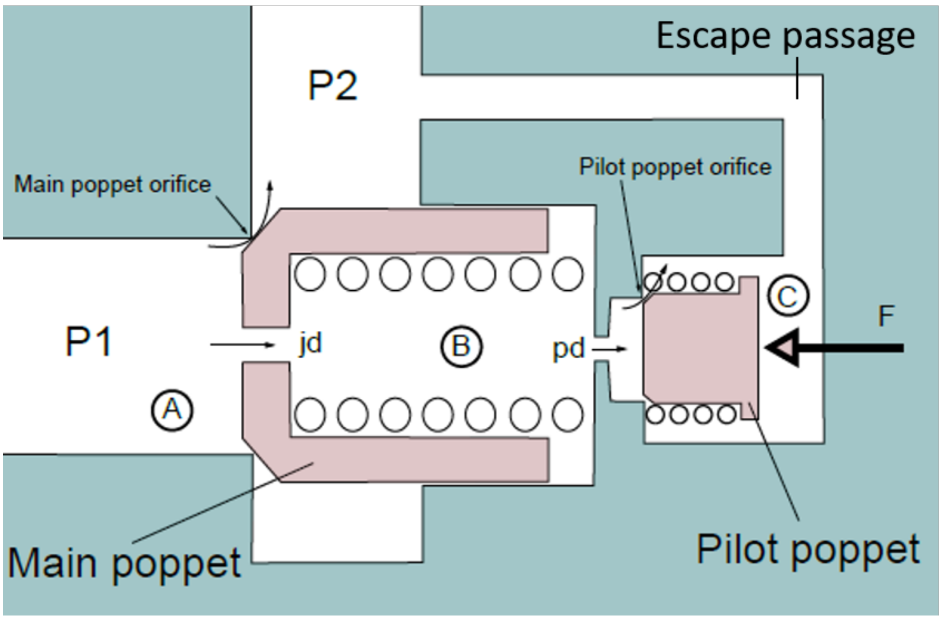

Figure 1.3.: Simplified function of a pressure regulating hydraulic valve

1.2. Problem Description

CES8700 is the fourth generation external valve designed by Öhlins. The manufacturing cost of CES8700 is rather high. A contributing factor is the manufacturing processes possibilities are limited by the requirements of fine dimensional tolerances of multiple components within the valve. Two components, which are major contributors to an increased manufacturing cost, are the armature and the valve body, see Figure 1.4. The armature and the valve body are assembled with a critical press fit. Both components require machining to achieve its fine tolerances that enables the desired press fit.

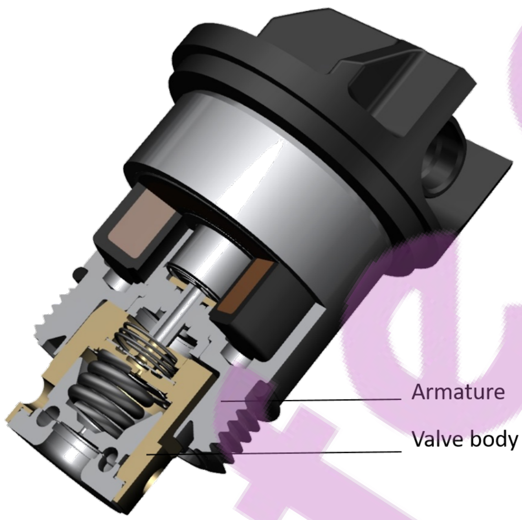

Figure 1.4.: Cross-sectional view of CES8700 displaying the armature and the valve body

In addition to the manufacturing process of the valve body, the component requires milling to create the escape passage. An escape passage is required to enable the hydraulic flow, which passes through the pilot stage, to reunite with the main flow within the damper. The escape passage is non symmetrical which prevents a symmetrical press fit, which is not optimum at higher loads. The press fit is crucial as it has a direct impact of the function of the valve. No interference of the press-fit prevents an assembly of the valve body. A too large interference deforms the inner surface of the valve body or dislocating the threads of the armature. A deformed inner surface of the valve body prevents the main poppet to move as it slides on the inner surface of the valve body. A stuck main poppet eliminates the pressure regulation, making the entire valve useless. A weak interference is there for desirable. Öhlins currently achieves a weak press fit with no critical deformation of the surfaces by several design parameters.

- Öhlins has designed the valve body with a portion of additional thickness where the press fit is located. The added material thickness prevents the press fit to easily deform the inner surface of the valve body. The surface of the additional material thickness is manufactured with extremely fine tolerances, to achieve the desired press fit. As the surface of the additional material is rather small, it prevents the entire valve to be manufactured with fine tolerances, see Figure 1.5.

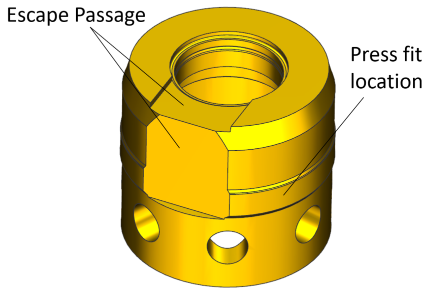

Figure 1.5.: Isometric view of valve body

- The armature is manufactured with an additional slim wall of material which deforms when press fitted. The material is locally deformed, which prevents the threads to dislocate during assembly. The surface of the deformed material is manufactured to achieve extremely fine tolerances, see Figure 1.6.

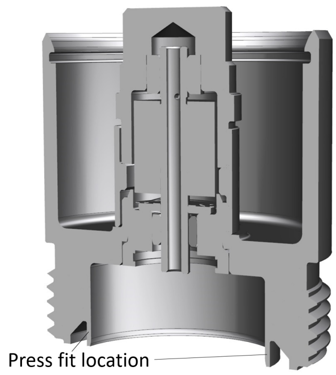

Figure 1.6.: Sectional view of the armature displaying the press fit location

Öhlins Racing now wants to evaluate the possibility of an additional solution, which is more cost efficient than the current solution. A solution that allows cheaper manufacturing processes of the armature and valve body by enabling coarser dimensional tolerances of the components. Öhlins suggest that a spring element between the valve body and the armature is a possible solution that should be investigated. An additional component usually increases the cost. However, a component which minimizes the impact of coarser tolerances and removes the milled escape passage could potentially minimize the cost by allowing cheaper manufacturing methods. A cheaper product minimizes the cost difference between passive and semi-active suspensions, while its increasing the cost difference to fully-active suspensions. This makes semi-active suspension technology more competitive on the market.

1.2.1. Requirements

1. The spring element must enable coarser tolerances of the armature and the valve body.
2. The spring element must enable a symmetrical press fit.
3. The spring element must allow an effective manufacturing.
4. The spring element must be easily assembled.
5. The spring element must be able to be manufactured using deep drawing process.
6. The spring element must prevent the valve body or the armature from dislocating during transport or mounting.
7. The height of the entire valve must remain constant.
8. The width of the entire valve must remain constant.
9. The spring element must enable an escape passage of the pilot stage.
10. The escape passage of the spring element must not result in pressure drop within the pilot stage.
11. The press fit must not critically deform the threads of the armature or the inner surface of the valve body.

1.3. Purpose and Aim

The purpose and aim of this bachelor thesis are to design and evaluate the feasibility of spring elements. The following issues will be answered throughout this report:

- How should the spring element be designed to meet the requirements?
- How should the solid mechanics of the spring element be evaluated?
- Which material is suitable for such spring element in such conditions?

1.4. Delimitations

The evaluation of spring element concepts will be evaluated using structural finite element analysis, i.e. no fluid dynamics simulations or prototypes assembled with valves will be performed. No simulation of deep drawing process of the final concept will be conducted in this thesis. Inner bend radius of the concept has been modeled with an even material thickness. Deep drawing process may cause dilution of bend radius which has not been taken into account. A simple evaluation if the concept is able to be manufactured using deep drawing process will be performed instead, taking no stress or strain limit into account. Only one concept will be evaluated using finite element analysis. No detailed cost-estimate will be carried out in this report. The result of this thesis will provide material for future studies of a detailed cost-estimate.

1.5. Outline

The theoretical background in Chapter 2 presents relevant basic theories to provide knowledge of how the concepts should be dimensioned, designed and evaluated. Methods are presented in Chapter 3 with accompanying simulation models. Evaluation and numerical results of the concepts are presented in Chapter 4. Thorough analysis of the final concept is located in Chapter 5. The report ends with discussion and conclusions in Chapter 6.

2. Theory

Chapter 2 defines and describes relevant theoretical areas as which the knowledge is a foundation of solving the problem.

2.1. Connection Between Problem and Theories

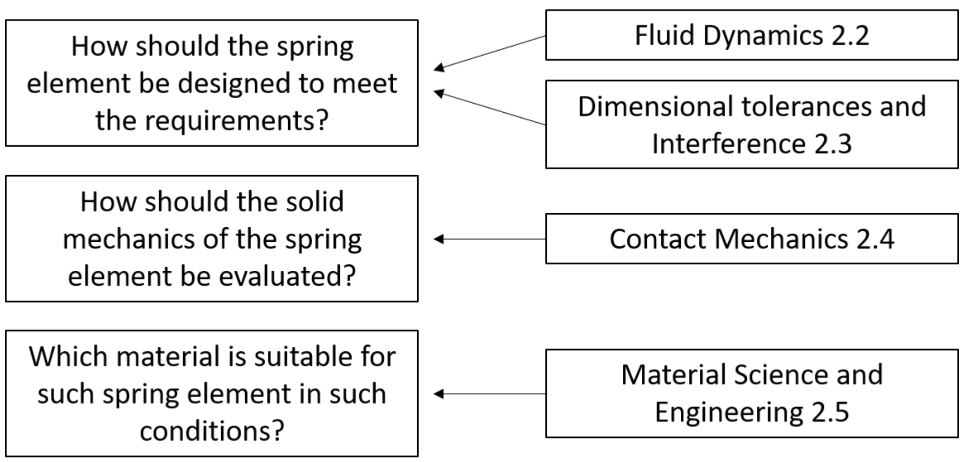

Figure 2.1.: Overview of which theoretical foundations contributed a solution to the problem within this thesis

The theoretical foundation of fluid dynamics is essential to meet the requirement of preventing a pressure drop. The theory thereby provides guidelines of how the escape passage should be designed.
The theory of dimensional tolerances and interference provides a foundation of the dimensions the spring element should have. The theory also presents a casual relation between tolerances and manufacturing cost.
When selecting a FEA-method to evaluate the solid mechanics of the spring element, it is important to understand the problem and under which conditions the spring element is exposed to. The used simulation model solves the contact problem using contact mechanic methods which makes the understanding of contact mechanics theories relevant.
Theory of material science provides important material properties that are relevant when selecting a material.

2.2. Fluid Dynamics

Bernoulli's equation in fluid dynamics expresses the energy of incompressible fluids i.e., the fluid density is constant and in frictionless flow at the coordinate s. Daniel Bernoulli stated, in such conditions, that the fluid pressure p_s, kinetic energy $\frac{1}{2}\rho u_s^2$ and potential energy $\rho g z_s$ correlates. Bernoulli published his principle in his book Hydrodynamic in 1738.
In incompressible fluid conditions, the total energy equation remains constant according to equation 2.1 [5].

$$p_s + \frac{1}{2}\rho u_s^2 + \rho g z_s = \text{constant} \tag{2.1}$$

Due to 2.1, the energy at two points on a streamline will be the same. The principle can be utilized by using two points1 & 2 on a streamline to extract unknown values according to the equation 2.2.

$$p_1 + \frac{1}{2}\rho \bar{u}_1^2 + \rho g z_1 = p_2 + \frac{1}{2}\rho \bar{u}_2^2 + \rho g z_2 \tag{2.2}$$

If we assume the system is incompressible, if there is no change in potential energy i.e. the relation of two points distance to a reference level is zero and if no pressure drop is allowed, the kinetic energy in point 1 must be larger than the kinetic energy in point 2 according to the equation 2.3.

$$p_2 \geq p_1,$$

$$\Delta \rho g z = 0,$$

$$\rho_2 - \rho_1 = 0,$$

$$p_1 + \bar{u}_1^2 = p_2 + \bar{u}_2^2 \tag{2.3}$$

By using the continuity equation of fluids, the velocity $\bar{u}$ of the fluid can be determined by the cross-sectional area A according to equation 2.4.

$$A_1 \bar{u}_1 = A_2 \bar{u}_2 \tag{2.4}$$

To prevent a pressure drop within the system, A_2 must be greater than A_1 to achieve a greater fluid velocity of point 1.

2.3. Dimensional Tolerances and Interference

A nominal dimension of a model in CAD-environment will not be fully achieved when manufactured. The absolute dimension of the manufactured model is determined by the accuracy of the manufacturing method. This must be taken into consideration when designing a component. The designer determines the allowed deviation of the nominal dimension. The acceptable deviation within the maximum and minimum dimensions is called tolerances. Different areas requires different tolerances and it's a critical decision due to the tolerance accuracy directly impacts the cost. The cost factor elevates exponentially as the accuracy of the tolerance widths increases, see Figure 2.2. Manufacturing method, tools and scrapping are a few factors that affects the exponentially growth of the increased cost.

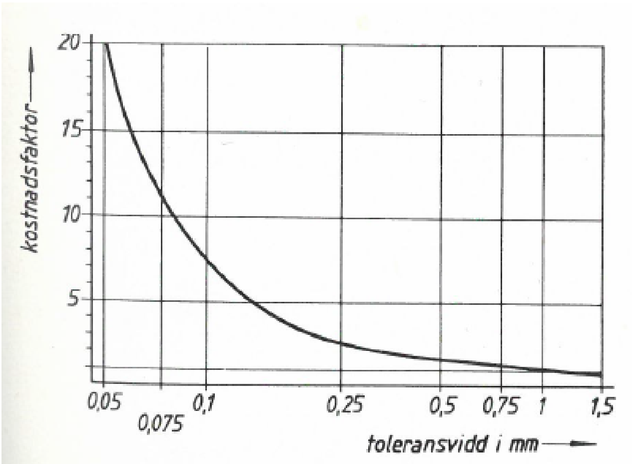

Figure 2.2.: Tolerance widths (x-axis) and cost factor (y-axis). Adopted from [2]

Engineering fit is defined by the dimensional difference of two assembled components. Engineering fit can result in two cases, interference or clearance. Interference is created when the cross sectional area of a shaft is larger than the diameter of a hole. Clearance occurs if the hole diameter is greater than the shaft diameter. When calculating, interference and clearance are defined as grip $\bar{g}$ according to equation 2.5.

$$\bar{g} = \bar{d}_h - \bar{d}_a \tag{2.5}$$

Interference fit can be assembled using two different methods, by using bonded press fit or bonded shrink fit. To create an interference fit, the shaft diameter must be greater than the hole diameter. Press fit are assembled by applying a force which forces the shaft into the hole. The weakest material of the components will slightly deform but without losing the fit characteristics. The shrink fit is assembled by either cooling the shaft, which will result in shrinkage, or by heating the hole, which will result in expansion of the hole. As either parts are experiencing dimensional changes due to change in temperature, they are forced together. The parts will return to their normal dimensions as they are no longer exposed to thermal conductivity and will generate an interference fit.

2.4. Contact Mechanics

Contact mechanics studies the deformation and stresses of a solid which is in contact with another solid. The following formulation of contact mechanics applies if one solid is a fixed rigid body.
The conditions of a contact system are defined by Signorini's contact conditions [6]. The potential energy of the system in function of a displacement vector is defined by

$$\Pi(\boldsymbol{d}) = \frac{1}{2}\boldsymbol{d}^T\boldsymbol{K}\boldsymbol{d} - \boldsymbol{F}^T\boldsymbol{d}, \tag{2.6}$$

where $\mathbf{K}$ is the stiffness matrix and $\mathbf{F}$ is the external nodal force vector. The difference of the elastic energy within the system and the external work results in the potential energy within the system. The stage as which the lowest potential energy within the system is the same stage which satisfies equilibrium.

$$\min_{\boldsymbol{d}} \Pi(\boldsymbol{d}) \tag{2.7}$$

Lowest potential energy within the system is defined by

$$\nabla\Pi(\boldsymbol{d}) = \boldsymbol{K}\boldsymbol{d} - \boldsymbol{F} = 0 \tag{2.8}$$

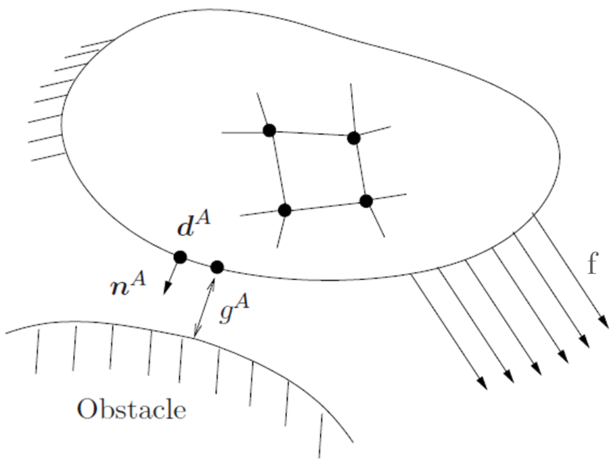

Figure 2.3.: Elastic body kinematic constrained by a fixed rigid obstacle. Adopted from [6]

An obstacle is presented to restrict the elastic body to deform freely. Kinematic constraints which prevents the body to penetrate the obstacle are defined by

$$\boldsymbol{d}\boldsymbol{n} - g \leq 0, \tag{2.9}$$

where $\boldsymbol{d}$ is displacement vector, $\boldsymbol{n}$ is normal direction vector of contact and g is distance to the obstacle in normal direction. The equation must be less or equal to zero to meet the constraints i.e. the distance to the obstacle must be greater or equal to the dislocation to have an operating contact. The kinematic constraints can be defined for all contacts nodes by

$$\boldsymbol{C}_N \boldsymbol{d} - \boldsymbol{g} \leq 0, \tag{2.10}$$

where $\boldsymbol{C}_N$ is a transformation matrix of $\boldsymbol{n}$ and $\boldsymbol{g}$ is a vector of all initial gaps g.
The kinematic constraints can be included in the equilibrium principle of the contact problem, i.e.

$$\begin{cases} \min\limits_{\boldsymbol{d}} \Pi(\boldsymbol{d}) \\ \text{s.t. } \boldsymbol{C}_N \boldsymbol{d} - \boldsymbol{g} \leq 0 \end{cases} \tag{2.11}$$

The optimal solution of constrained optimization problems are given by Karusch-Kuhn-Tucker conditions (KKT-conditions):

$$\begin{cases} \boldsymbol{K}\boldsymbol{d} - \boldsymbol{F} + \boldsymbol{C}_N^T \boldsymbol{P}_N^A = 0 \\ \boldsymbol{P}_N^A \geq 0 \\ \boldsymbol{C}_N \boldsymbol{d} - \boldsymbol{g} \leq 0 \\ \boldsymbol{P}_N^A \circ (\boldsymbol{C}_N \boldsymbol{d} - \boldsymbol{g}) = 0 \end{cases}, \tag{2.12}$$

where $\boldsymbol{P}_N^A$ is the contact force in normal direction of the contact. The formulation of this problem is called Lagrange formulation. A central distinction of Lagrangian formulation is that it treats the conditions as additional equations and lagrange multipliers $\boldsymbol{P}_N$ are interpreted as contact forces. The first condition of the lagrange formulation defines the equilibrium state of the system which is given by Signorini's contact conditions combined with the contact force. The remaining conditions are given by KKT-conditions. The first condition of KKT-conditions states that the contact force must not be negative. The second KKT-condition states that the contact distance must be greater or equal than the displacement in normal direction i.e. the body can not penetrate the obstacle. The third and last condition states that if there is no contact, the contact force must be zero. The last condition also states that if there is contact, the contact force must be greater than zero.

Commercial FEA softwares approaches contact problems with an augmented formulation of Lagrangian combined with either Uzawa's or Newton's method. An augmented Lagrangian formulation includes the expression of which stage equilibrium is satisfied and an equivalent formulation of Signorini's condition, which is defined by

$$\begin{cases} \max\limits_{P_N^A} \left(d_N^A - g^A\right) P_N^A \\ s.t.\ P_N^A \geq 0 \end{cases} \tag{2.13}$$

The contact force P_N^A is equivalent to projection defined by

$$\begin{cases} P_N^A = \left(P_N^A + r\left(d_N^A - g^A\right)\right)_+ \\ \text{where } \mathbb{R}_+ = \{x : x \geq 0\} \end{cases} \tag{2.14}$$

The foundation of Uzawa's and Newton's methods constitutes of the projection of the contact force defined in (2.14). [6]

2.5. Material Science and Engineering

Material selection is a critical part of product development as it has a direct impact of the performance of the product. Material selection can also enable that tough requirements of the product/component is met. It is essential that important material properties are prioritized in order to optimize the function of a product or component. Material properties can be categorized into general, mechanical, optical, thermal and electrical, just to mention a few. Important material characteristics regarding this thesis are defined below.

2.5.1. Engineering Stress and Strain

Stress, σ, within the material occurs when a force, F, is acting on the cross-sectional area, A, according to equation 2.15. Engineering stress does only account for the initial cross-sectional area, whereas the force can differentiate in a stress-strain curve.

$$\sigma = \frac{F}{A} \tag{2.15}$$

Strain, ε, is a result of an applied stress on the material. If the applied tensile or compressive stress is large enough, the material will either increase or decrease in length. Strain is defined by the change in length, Δl, divided by the original length, l_0, according to equation 2.16.

$$\varepsilon = \frac{l_i - l_0}{l_0} = \frac{\Delta l}{l_0} \tag{2.16}$$

2.5.2. Hooke's Law

Materials do not behave similarly when exposed to stress. A measurement of a material's ability to withstand changes in length when stress is applied was there for required to form a relationship. Young's modulus E, named after the 18th-century English scientist Thomas Young, defines such relationship. Hooke's law defines the relationship between stress-strain-young's modulus according to equations 2.17.[12]

$$E = \frac{\sigma}{\varepsilon} \tag{2.17}$$

2.5.3. Yield Stress

Elastic deformation refers to the ability of a material to return to its original form after being exposed to stress. If however, the applied stress is large enough, the material will undergo permanent deformation, also known as plastic deformation. The stress limit of elastic deformation is determined by the proportional point P, which is individual for each material. The proportional point P is defined by the initial divergence from linearity of the stress-strain curve. The initial divergence is very difficult to define and as a consequence, yield stress/strength has been introduced. The yield stress of a material is defined by the offset method. The method constructs a parallel line to the linear stress-strain curve with an offset of 0.2% strain. The stress corresponding to where the constructed line intersects with the stress-strain curve is defined as the yield stress, or the yield strength of a material, see Figure 2.4. As 0.2% strain is almost negligible, the yield strength σ_y is often referred to the stress limit which a material can withstand without plastically deform. [12]

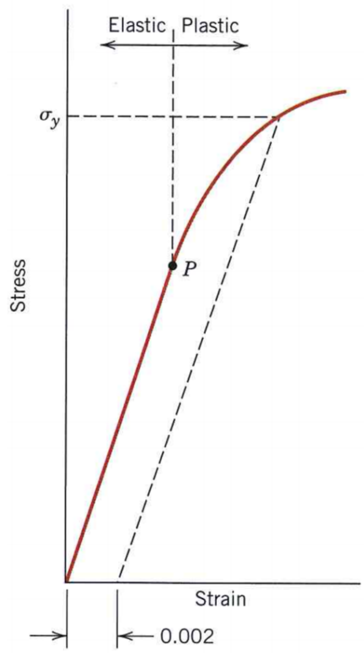

Figure 2.4.: Stress-strain curve with offset-method. Adopted from [12]

2.5.4. Strain Hardening

Strain hardening, or work hardening, is the hardening which increases the strength and decreases the ductility of a material which experience strain. Strain hardening can be defined in an engineering stress-strain curve or in a true stress-strain curve. An engineering stress-strain curve is designated by the computation with a constant area. A constant cross-sectional area generates a curve which displays that no additional stress is required to fracture as the stress reached the material's ultimate tensile.

A true stress-strain curve defines stress and strain accordingly,

$$\sigma_{true} = \frac{F}{A_i} \tag{2.18}$$

$$\varepsilon_{true} = \ln(\frac{L_i}{L_0}) \tag{2.19}$$

True stress and strain can be defined in relation to engineering strain can be expressed according to the definitions 2.20 & 2.21,

$$\sigma_{true} = \sigma(1+\varepsilon) \tag{2.20}$$

$$\varepsilon_{true} = \ln(1+\varepsilon) \tag{2.21}$$

The definition of stress and strain separates the true and engineering approach. True stress and true strain takes the instantaneous values of the cross-sectional area A_i and the length l_i into account according to the definitions expressed in eq 2.18 and equation 2.19. The engineering stress-strain only considers the original cross-sectional area for stress and the final strain for strain. The result of this is two different looking stress-strain curves whereas true stress-strain will be conducted in this thesis, see Figure 2.5.

Strain hardening occurs as the stress exceeds the yield stress. The material plastically deformations at stresses higher than the material's yield strength. Plastic deformation permanently deforms the material, previously called strain hardening. The stress-strain relation of strain hardening can be displayed using a tangent modulus. Tangent modulus can be defined as bilinear or multilinear. A bilinear tangent modulus consists of only one linear tangent between two points. Multilinear consists of several linear tangents. Bilinear tangent modulus can be useful when the strain hardening behavior is unknown but e.g. yield stress and Ultimate tensile stress is known.

To calculate the tangent modulus between the point of yield stress and the point of ultimate tensile stress, four coordinates are required. σ_y yield stress, ε_y strain at yield stress, $\varepsilon_{UTS_{true}}$ strain at true ultimate tensile stress and $\sigma_{UTS_{true}}$ true ultimate tensile stress. The coordinates are obtained accordingly,

$$\sigma_y = Given\ value\ of\ yield\ stress\ [MPa]$$

$$\varepsilon_y = \frac{\sigma_y}{E}$$

$$\varepsilon_{UTS_{true}} = \ln(1 + \frac{elongation\%}{100})$$

$$\sigma_{UTS_{true}} = \sigma_{UTS}(1 + \varepsilon_{UTS_{true}})\ [MPa],$$

where E is the Young's modulus. The slope of the tangent modulus can then be calculated by equation 2.22,

$$E_t = \frac{(\sigma_{UTS_{true}} - \sigma_y)}{(\varepsilon_{UTS_{true}} - \varepsilon_y)} \tag{2.22}$$

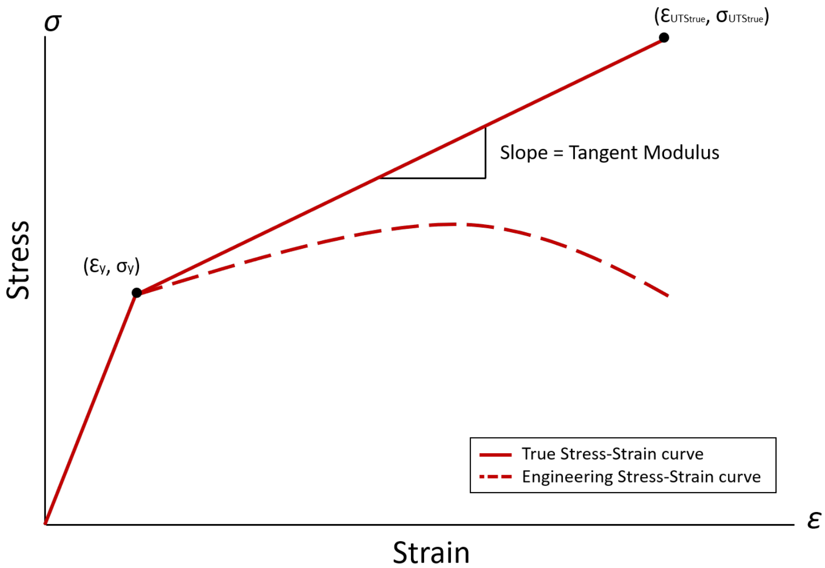

Figure 2.5.: True Stress-Strain curve and Engineering Stress-Strain curve comparison and accompanying explanation of bilinear tangent modulus

When a stress larger than the yield strength of a material is removed, partial elastic recovery of the total deformation will occur. The result of plastic deformation will not affect the material's ability to still elastically deform, but as an already plastically deformed material. The amount of strain a material can experience is determined by the ductility of a material.

2.5.5. Ductility

Ductile materials can deform to a certain rate without fracturing. Ductile materials are favorable when the design of the component requires forming operations. Ductility is defined in percent as elongation according to the equation 2.23.

$$\%EL = \left(\frac{l_f - l_o}{l_0}\right)100 \tag{2.23}$$

The opposite of ductile is brittle. The atoms in brittle materials are bonded and structured in such way to prevent strain. Fracture in brittle material can there for be sudden and unexpected, see Figure 2.6. [12]

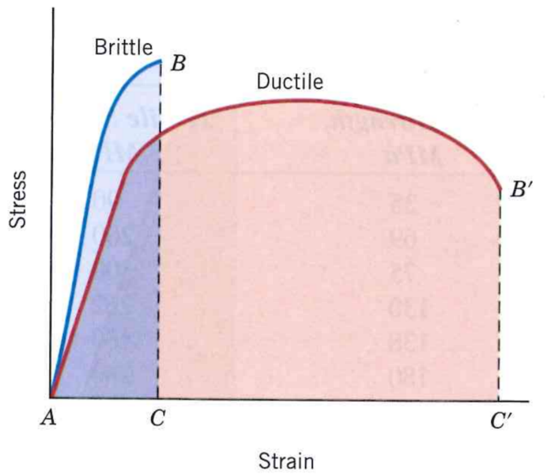

Figure 2.6.: Characteristics of a brittle and ductile material in a Stress-strain curve. Adopted from [12]

3. Method

This chapter provides an overview and a description of the carried out method used to achieve a valid result.

3.1. Concept and Evaluation Study

The objective of this thesis was to design and evaluate spring element based of given requirements. Concepts were generated and then screened to obtain a final concept which had the most potential to meet each requirement. The final concept was then evaluated using finite element analysis.

3.1.1. Finite Element Analysis

The finite element method (FEM) is a numerical method used to perform finite element analysis of any given physics problem. Typical physics problem includes structural analysis, heat transfer, fluid flow and electromagnetic potential. The problems can be defined in partial differential equations (PDE). To be solved, the analytic solution requires boundary values of the PDE, which are rarely obtained. Finite element formulation consists of a system of algebraic equations instead. To simplify the solution of the system consisting of unknown numerical values, it is subdivided into smaller systems also known as finite elements. Finite equations consisting of numerical values simplifies the calculations, but the number of equations to solve is increased. By utilizing the computation time of a computer, the system can be solved effectively, which is performed in several modern softwares. The solution of each equation can then be assembled into a larger system which defines the entire problem.[3]

Finite element analysis is performed in this thesis to find the solutions regarding the given requirements. The solutions determined if the spring element met each requirement.

3.2. Validity and Reliability

Validity is achieved by performing a finite element analysis, which is a commonly used method to obtain results of stresses, strains and reaction forces in a given problem. Reliably results are achieved by simulating worst cases which represents scenarios with the least favorable parameters such as, dimensions, material properties and friction coefficients. A mesh independence study is performed to achieve a mesh which provides a result with high accuracy. Contacts are analyzed using Contact Status to ensure no significant interpenetration of surfaces would occur.

4. Analysis

A thorough presentation of the simulation analysis will be conducted in Chapter 4.

4.1. ANSYS Workbench

The finite element analysis in this thesis was performed using ANSYS Mechanical 18.2. The simulation consisted of three components, the spring element concept, the armature and the valve body. Symmetrical planes were evaluated of each component's geometry to simplify the simulation and decrease the time required to solve the problem. ANSYS consists of multiple analysis systems, which is chosen depending on the problem. Static structural is an analysis system which was chosen for the problem in this thesis. Static structural determines stresses, strains and reaction forces caused by steady loading i.e., loads that with respect to time varies slowly. Static structural allows linear or nonlinear behaviors, example of nonlinearity behaviors are large deflections, plasticity, friction coefficient and contacts. This thesis consisted of a nonlinear contact problem which was solved using an implicit solver. The solver consisted of an unsymmetrical Newton-Raphson method.

ANSYS allows multiple number of load steps. Each load step has a virtual time unit of 1. Each load step also consists of points at which solutions are computed, in ANSYS these points are called substeps. The amount of substeps can manually be controlled to obtain convergence. Convergence occurs when the residual, the difference between the external and internal force, is less than the convergence criterion. Error is inherent in nonlinear analysis, convergence criterion is basically the allowance of error, usually in percentage.

4.2. Changes of Armature and Valve Body

Unaffected material was removed from the armature and the valve body to simplify the simulation, see Figure 4.1 & 4.2. Dimensional changes of the armature and the valve body were also performed to allow an assembly of an additional component to prevent an increased length or height of the entire valve. Dimensional changes of the armature were an increased inner diameter of the interface and height removal. The diameter was gradually increased to ensure that there was no dislocation of the threads. A greater dimensional interface of the armature allows for additional dimensional freedom of the spring element. To prevent an increased height of the valve with an assembled spring element, the interface was also designed 0.5 mm deeper, which corresponds to the additional height caused by the material thickness of the spring element. The outer surface of the simplified armature was dimensioned equally to the lowest dimensional diameter of the threads, to not add a false material thickness.

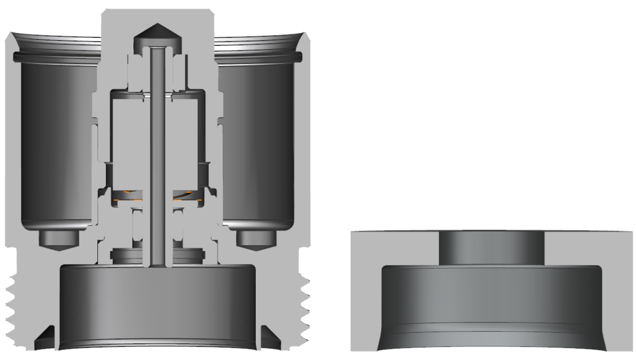

Figure 4.1.: Sectional view of the original armature design (left) compared to the simulated armature (right)

Greatest dimensional changes of the valve body were reduction in height, removal of escape passage and simplification of the material thickness, see Figure 4.2. The material thickness was reduced to the lowest value while maintaining the original design. This was performed to achieve a sensitive result whether the inner surface of the valve body would be deformed.

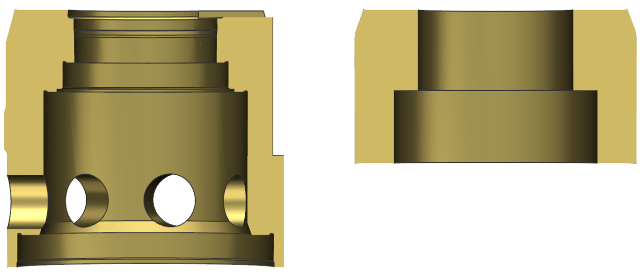

Figure 4.2.: Sectional view of the original valve body design (left) compared to the simulated valve body (right)

4.3. Geometry Optimization

Symmetry planes of the simulation model and removal of unaffected material were utilized to minimize the required computer storage and required CPU time. It was critical to minimize these loads to achieve efficiency while providing enough accuracy of the solution. Minimizing the computer storage of the simulation files and the required CPU time are also essential if additional capacity can not be provided.

The simplified armature and valve body were uniform around Z-axis and could have enabled a 2D simulation. By the design of the spring element concept, the simulation required to be in a 3D-environment since it was not uniform around Z-axis. The final concept of the spring element was optimized with symmetry planes by 1/4 of the original model, see Figure 4.3.

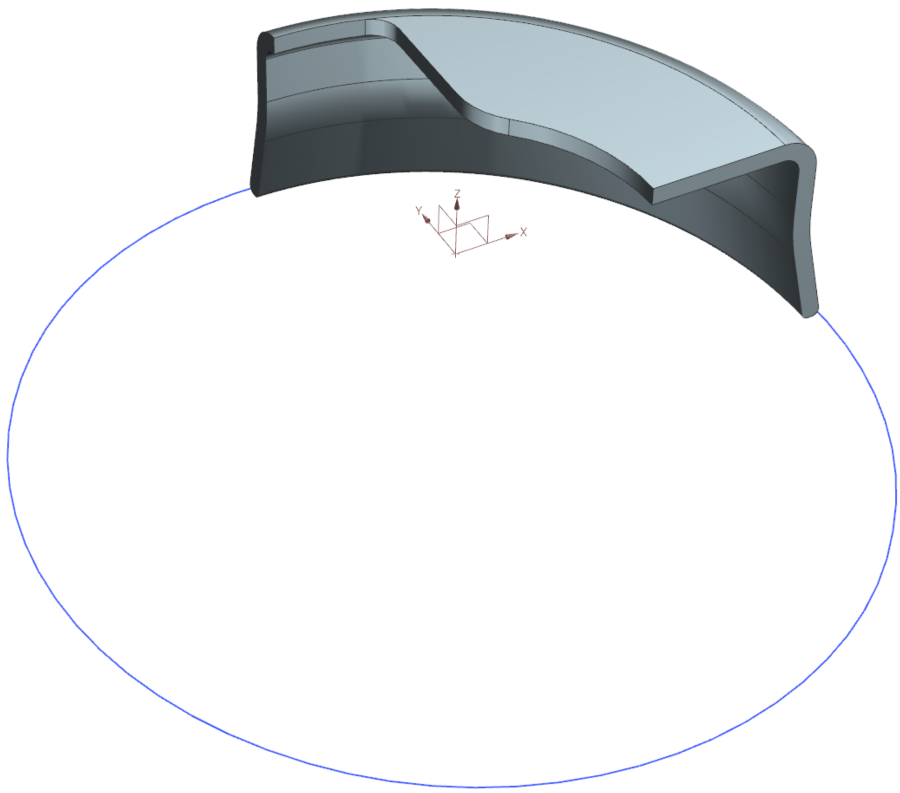

Figure 4.3.: By utilizing symmetry planes, the simulation model of the final concept was reduced to 1/4 of it's original size

Symmetry settings in ANSYS enables the behavior of a fully scaled assembly in a downscaled model. Validation of the downscaled model was performed with a simple load which was compared to a fully scaled model which also was exposed to the same load. The result displayed equal behavior and values, which ensured a correct downscaled model.

4.4. Assembly and Disassembly Simulation

An assembly and disassembly simulation were performed to locate maximum stresses, strains and reaction forces. Maximum stresses, strains and reactions forces were critical values that would determine if the spring element would meet several requirements. Maximum stresses determined if the design and material of the concept were good enough. An analysis of strains would provide data if the crucial surfaces were critically deformed during the assembly. Resulting reaction forces during the simulation provided which assembly and disassembly forces were required. The simulation model was assembled and disassembled using displacements. In ANSYS, displacements are boundary conditions in static structural which displaces a chosen part within the model. Reaction forces are obtained as a displaced component is in contact with another component. The components were displaced in a specific order that allowed for a similar assembly in production. The boundary conditions were also set to enable both assembly and disassembly in one simulation.

The starting position is displayed in Figure 4.4a. In the first load step, the concept was displaced 1.99 mm which presses the concept onto the valve body but leaves a gap of one hundredths mm, which is performed to prevent interpenetration of the inner upper surface of the concept and the outer upper surface of the valve body. The concept was fixed at this position until the last load step. The valve body was fixed during all load steps except the last. In the second load step, the armature was displaced 3.99 mm which was equal to the distance required to press the armature onto the concept and valve body. All parts were in position after the second load step i.e. the assembly was complete, see Figure 4.4c. The disassembly of the model was performed at the fourth load step. The disassembly was performed by displacing the valve body 2 mm. The concept was no longer fixed at the fourth load step, which resulted in a release of the weakest press fit as the valve body was displaced, see Figure 4.4d. Figure 4.4 displays the assembly and disassembly when the press fit of the armature and concept was the weakest.

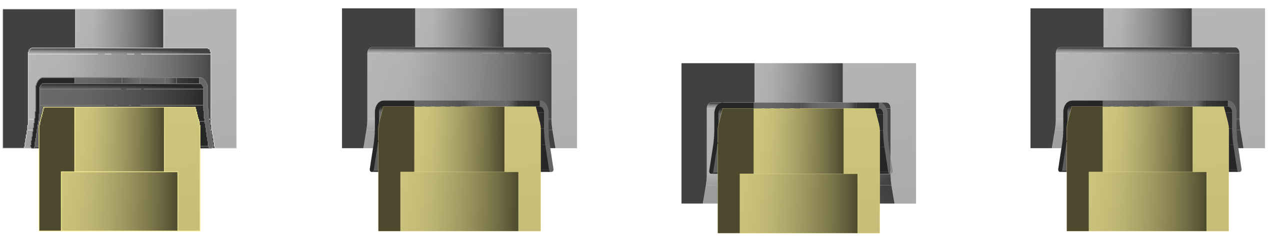

(a) Starting position (b) After first load step (c) After second load step (d) After third load step

Figure 4.4.: Worst case 1 representation of assembly and disassembly of the model by each load step

An additional scenario, which is defined as Worst Case 2 further in this thesis, would occur as the press fit of the valve body and the concept would be the weakest. This resulted in the concept remained it position with the armature as the valve body was displaced 2 mm, see Figure 4.5d. The cause and purpose of this will be explained thorough in Section 4.5

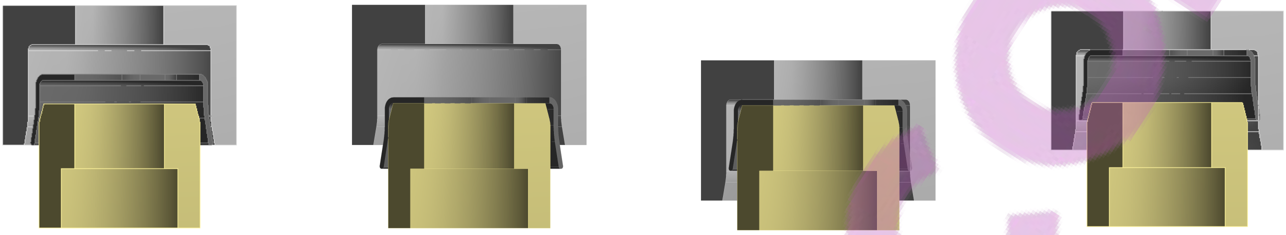

(a) Starting position (b) After first load step (c) After second load step (d) After third load step

Figure 4.5.: Worst case 2 representation of assembly and disassembly of the model by each load step

To achieve a valid result of the assembly and disassembly simulation, the model was required to move freely in Z-direction but locked in X- and Y-axis to prevent rotation around Z-axis. This was performed taking production into consideration as no rotational movement would occur during production assembly. A boundary condition that met such requirements was frictionless support. The frictionless support was applied on the faces in X- and Y-axis of the model, see Figure 4.6.

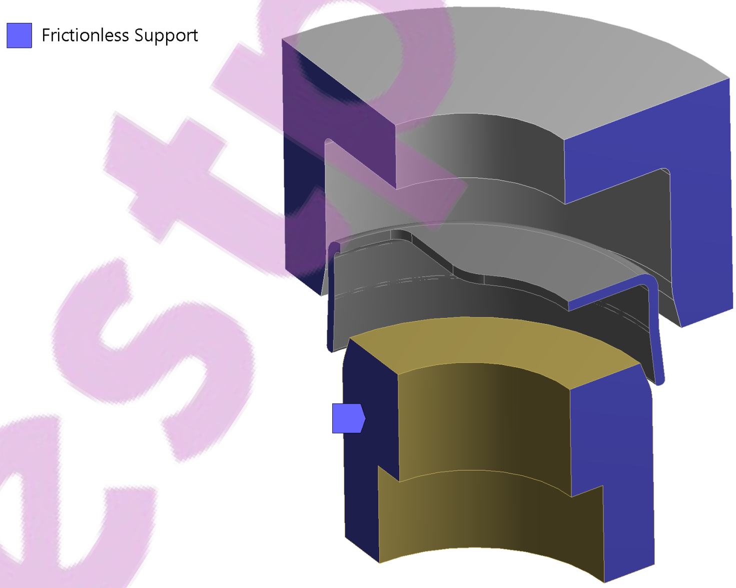

Figure 4.6.: Frictionless support applied in x and y-direction of the model to prevent rotational movement

4.5. Dimension and Tolerance Evaluation

The dimension of the components was defined as grip, to reduce the parameters from three dimensions to two grips. Grip size allowance corresponds to press fit capacity allowance and was determined by an interval of maximum and minimum grip. Minimum grip was defined by the grip resulting in a disassembly force just above an insufficiently low value. Maximum grip was defined by the grip resulting in a maximum stress within the model just below the ultimate tensile strength (UTS_{true}) of any material, see Figure 4.7. To achieve dimensions resulting in grips within the interval, trial and error simulations were performed.

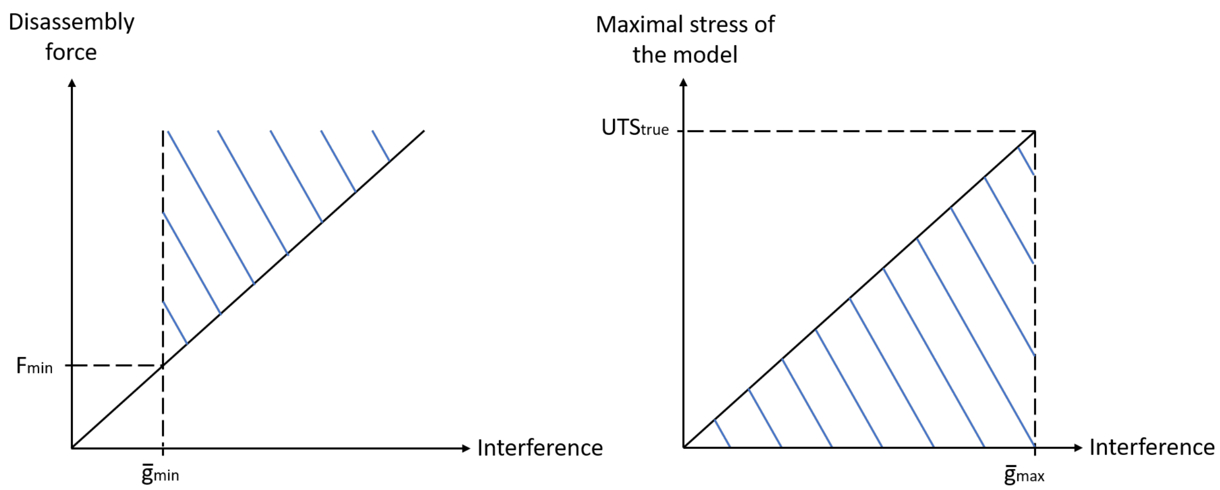

Figure 4.7.: The allowed range (blue striped) of interference in relation to disassembly force and maximum stress

The trial and error simulations resulted in partial counteracting press fits. Counteracting press fits were defined as one press fit was reduced as the other was increased. To evaluate tolerance width allowance, worst cases were then created. Worst cases were modeled by components dimensional extremes, which included tolerance widths, to achieve the least favorable combinations. Least favorable combinations of counteracting press fits were achieved by using dimensions and tolerance extremes which caused one maximum grip and one minimum grip.Dimensions of the components were to be determined (TBD). The typical dimensional tolerance ± 0.05 mm of the spring element concept was obtained by Öhlins component supplier which was applied for deep drawing process, see Table 4.1. This was performed to evaluate if the concept would allow coarser tolerances of the armature and the valve body and if it would prevent dislocation of either the valve body or the armature during transportation or production assembly.

Component	Armature	Spring Element Concept		Valve Body
Measurement	Interface Ø	Absolute outer Ø	Absolute inner Ø	Absolute outer Ø
Dimension Worst Case 1	TBD + (TBD)	TBD - (0.05)	TBD - (0.05)	TBD + (TBD)
Dimension Worst Case 2	TBD - (TBD)	TBD + (0.05)	TBD + (0.05)	TBD - (TBD)

Table 4.1.: Dimensional combinations to achieve worst cases

Press-fit	A - C	VB - C
Interference Worst Case 1	$\bar{g}_{min}$	$\bar{g}_{max}$
Interference Worst Case 2	$\bar{g}_{max}$	$\bar{g}_{min}$

Table 4.2.: Worst cases presented as interferences

The tolerances which the spring element allowed were then extracted by the difference in dimension of each components max and min dimension. Nominal dimension of each component was given by the mean value of max and min dimensions.

4.6. Disassembly Force Evaluation

A value of the minimal allowed disassembly force wasn't stated in the requirement. The result of the disassembly force using spring element would therefore be compared to the total mass of the valve body assembly, M_{VB}, multiplied with the gravitational force, g. The valve body assembly's weight in $[N]$ is calculated in eq 4.1.

$$M_{VB} \cdot g = 0.031 \cdot 9.815 = 0.304\ N \tag{4.1}$$

4.7. Material Data

The armature is made out of carbon steel alloy which is a processed high carbon chromium bar. A high carbon chromium steel prevents oxidation and it allows cutting processes to achieve the required fine tolerances. The valve body is made of a brass-copper-zinc alloy. The material is easily machined which is essential to achieve the fine tolerances and milling of the escape passage.

The material of the concept had to be chosen before performing simulation the model. The system required material data of all component to compute the stresses and deformations. The material of the concept had to meet several requirements, which were enabling a deep drawing process and allowing great elastic and/or plastic deformation without fracturing. An additional important property was which friction coefficient the material would yield when in contact with the material of the armature and the valve body. A too high friction coefficient would yield high stresses within the materials but the required force to disassembly would potentially be high, which was desired. A too low friction coefficient would result in a potentially low disassembly force. A material that met the requirements was a steel manufactured by SSAB. The elongation of the steel was 34% which defines a highly ductile steel with potentials of meeting the material requirements of a spring element. Further material properties can be seen in Table 4.3. Friction coefficients of material combinations will be presented in Section 4.8.

Component	Concept	Valve body	Armature
Material	Steel alloy	Brass alloy	Steel alloy
Classification by manufacturer	SSAB Form 03	-	-
Young's modulus [GPa]	200	98	210
Poisson's ratio	0.3	0.3	0.3
Yield strength [MPa]	240	220	N/A
Elongation [%]	34	35	N/A
UTS [MPa]	270-370	400	N/A

Table 4.3.: Material data of the materials used for the Spring element, the valve body and the armature [10]. Material data of brass and steel alloy was obtained from Öhlins material supplier.

Isotropic elasticity was chosen in ANSYS material model of the armature's and the valve body's material. Isotropic elasticity model only takes materials elastic deformation into account. The material of the spring element concept would experience both elastic and plastic deformation to operate. Two different material models had to be used to enable both, which were isotropic elasticity and bilinear isotropic hardening. Bilinear isotropic hardening sets a linear plastic deformation hardening of the material. Bilinear isotropic hardening required the material's tangent modulus, which was calculated using the derivation presented in Chapter 2 Strain Hardening.

The material data from SSAB consisted of a range of engineering ultimate tensile strength, 270 - 370 MPa. The true ultimate tensile strength of SSAB Form 03 was calculated using the lowest value of the range (270 MPa), see Figure 4.8. Evaluation using the lowest value of UTS was used to increase the safety margin during a potential production. Linear plastic deformation was chosen because no true stress-strain curve was available and the plastic behaviour was unknown.

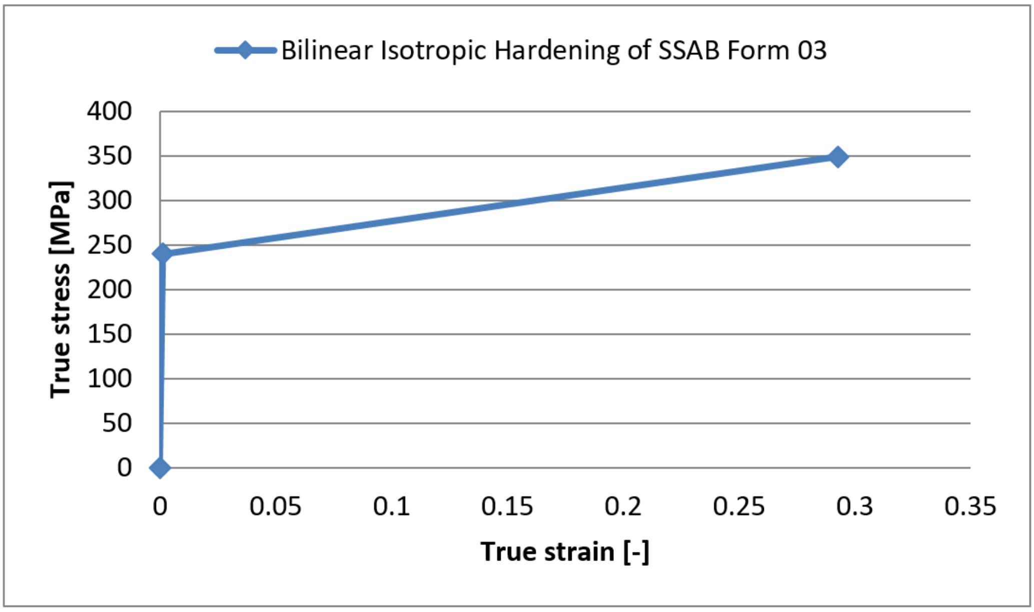

Figure 4.8.: True stress-strain curve of SSAB Form 03 including strain hardening

4.8. Contacts

A contact occurs as two different bodies shares the same boundary. Physical contacts do not interpenetrate the surfaces. In simulation environment, the system must there for enable settings to prevent the surfaces from interpenetrate. ANSYS offers several contact algorithms which enforces the contact behavior of physical contacts [1]. Contact settings in ANSYS allows the user to set several parameters in which the desired contact behavior is achieved. To achieve a simulation model with high reliability, the contact settings are critical.

Contact Type is a contact setting which defines the type of contact. Frictional contact takes frictional forces into account as sliding of the contact occurs. Contact sliding would occur during the assembly and disassembly and frictional forces would be generated. The model required static frictional coefficient of each contact to enable the computation of frictional contact. The frictional coefficient was determined by the materials which were in contact, but also by whether the contact surface of each material was dry or lubricated. The model consisted of a valve body, spring element concept and an armature which yielded two contacts, Brass - Steel (valve body and spring element concept) and Steel - Steel (spring element concept and armature). All components are manufactured and assembled with a clean and dry surface. Table 4.4 is a summarized table of friction coefficient of material combinations conducted in this thesis. Several simulations revealed that the disassembly force was the most critical parameter. To achieve the absolute worst cases of the disassembly forces, the lowest value of frictional coefficient was chosen of steel - steel contact, which would yield a lower disassembly force.

Materials and Material Combinations		Static Frictional Coefficient [μ_s]	
		Clean and dry surfaces	Lubricated and Greasy Surfaces
Brass	Steel	0.35	0.19
Steel	Steel	0.5 - 0.8	0.16

Table 4.4.: Friction coefficients of material combinations which are in contact [11][4]

Frictional Contact was applied on the outer surface of the valve body and the inner surface of the concept, see Figure 4.9. The frictional coefficient was set to 0.35 μ_s. *Frictional Contact* was also applied on the outer surface of the valve body and the inner surface of the armature, see Figure 4.10. The frictional coefficient was set to 0.50 μ_s.

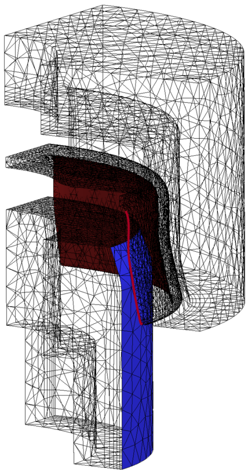

Figure 4.9.: Frictional contact of the outer valve body's surface and the inner concept's surface

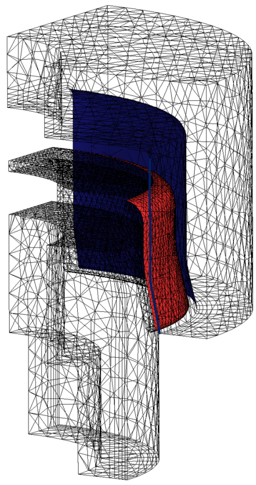

Figure 4.10.: Frictional contact of the inner armature's surface and the outer concept's surface

Frictionless Contact is a contact type which enables contact sliding without generating frictional forces. *Frictionless Contact* was applied on the upper outer surface of the valve body and the inner upper surface of the concept, this to prevent the surfaces to stick to each other, see Figure 4.11. *Frictionless Contact* was also applied on the outer upper surface of the concept and the inner upper surface of the armature, see Figure 4.12.

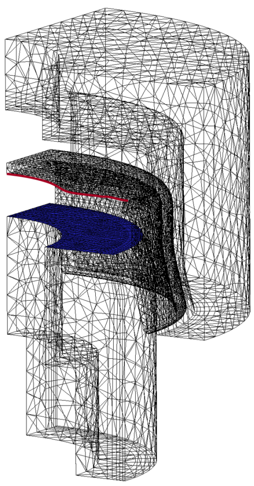

Figure 4.11.: Frictionless contact was applied of surfaces displayed in red and blue

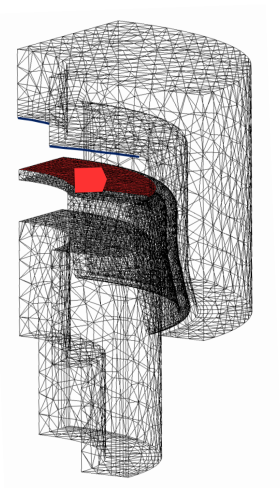

Figure 4.12.: Frictionless contact was applied on surfaces displayed in red and blue

Normal Stiffness Factor determines the stiffness of the contact springs, located at each node. *Normal Stiffness Factor* can be defined according to eq 4.2

$$F_{normal} = k_{normal} x_{penetration} \tag{4.2}$$

where F_{normal} is the finite contact force, k_{normal} is the contact stiffness and $x_{penetration}$ is the penetration of contact surfaces [1]. According to eq 4.2, an increase in contact stiffness would decrease the contact penetration. The solution would be accurate if the penetration was small or negligible. A stiffness factor of 10 was chosen, which was recommended for bulk deformations [7]. Contact springs which determines contact stiffness can be seen in Figure 4.13.

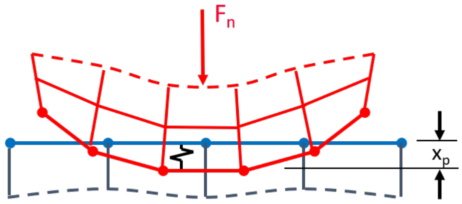

Figure 4.13.: Displays the relation of Contact force, Contact springs and penetration. Adopted from [1]

Additional contact settings were set to *Program Controlled*. *Program Controlled* property of each contact setting allows the program to set which property of each setting to be used based of its calculations. *Program Controlled* is set as the default property of each setting in ANSYS. List of all contact settings and each property can be found in [7].

4.9. Mesh

A mesh independence study has been performed to analyze the mesh influence of the results. Mesh independence study can be found in Appendix A.

The armature and the valve body were considered non-critical due to the high material thicknesses of the components. The armature and the valve body were assigned an element size of 1.00mm. Relevant values of stresses and strains of the non-critical components were expected to emerge just below contact surfaces. *Inflation layers* of the mesh model were applied on each contact surface of the non-critical components. *Inflation layers* provides user defined number of layers below a desired surface. *Inflation layers* enables a more accurate value of stresses and strains to be obtained close to surfaces using a coarse mesh of the entire model. Five inflation layers were applied on the armatures inner surface and the outer surface of the valve body, see Figure 4.14. A mesh of element size 0.33 mm was applied on the valve body's upper surface. No critical values of stresses or strains were expected on the surface, however a finer mesh was required for the model to perceive the contact between the valve body's upper surface and the spring element's inner-upper surface. The result of the final mesh of the model can be seen in Figure 4.14. The model consisted of 60238 nodes and 48351 elements total.

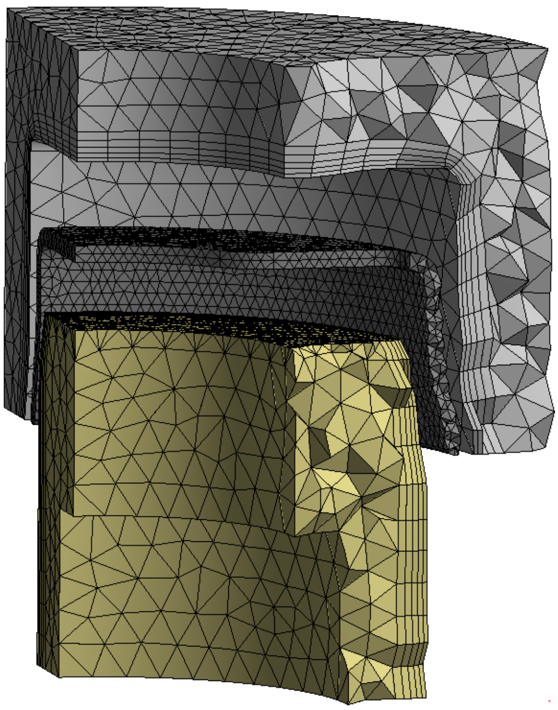

Figure 4.14.: Final mesh of simulation model showing whole elements at the right side

Element order of the mesh was set to *program controlled. Program controlled* element order enables different element orders within the mesh. ANSYS defines element orders by element descriptions. The model was given element descriptions SOLID186 and SOLID187.

SOLID186 is a quadratic element order. A SOLID186 element is defined by 20 nodes, each with three degrees of freedom. SOLID186 can be defined in several options displayed in Figure 4.15. A high order hexahedral element provides a highly accurate result due to increased number of nodes. Hexahedral element however causes an increased computation time and complicates the implementation within complex shapes. Hexahedral elements were implemented by using *inflation layers* setting of the contact surfaces. The mesh model also consists of a high order prism. This is to enable the transformation of element shapes hexahedral and tetrahedral. [8]

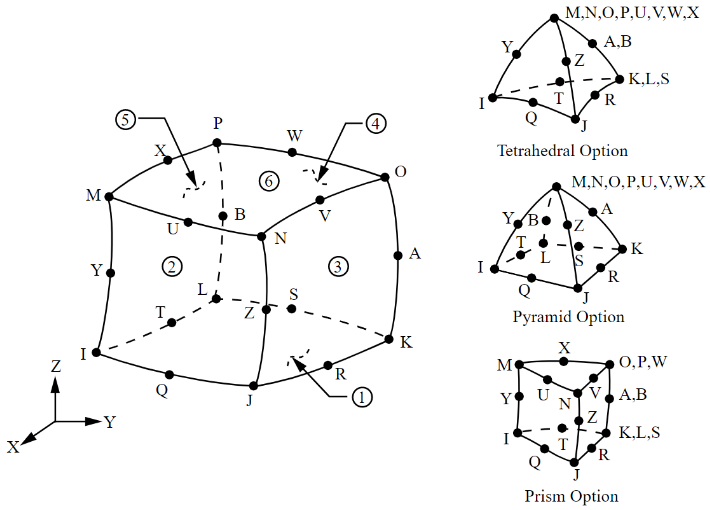

Figure 4.15.: Element description SOLID186. Adopted from [8]

SOLID187 defines a tetrahedral element with quadratic order, see Figure 4.16. The element consists of 10 nodes, each with three degrees of freedom. Compared to hexahedral elements, tetrahedral elements are more easily fitted into complex shapes and decreases the computation time due to lower number of nodes. Tetrahedral elements have been implemented of the body sized mesh of every component within the model. [9]

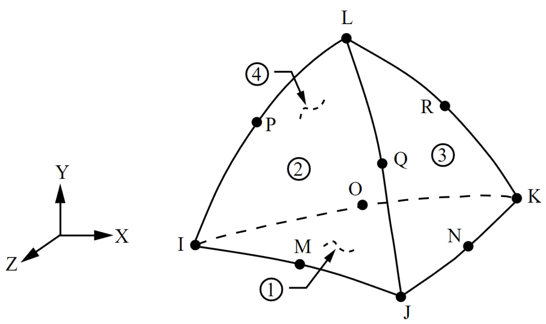

Figure 4.16.: Element description SOLID187. Adopted from [9]

4.10. Escape Passage Evaluation

Two methods were used to evaluate the escape passage capacity, since two different methods with a similar result increases the reliability of the result. The first method was performed by using the derivation expressed in Chapter 2 Fluid Dynamics. Two points were required i.e, two areas within a streamline as which the fluid behavior was studied. The derivation in Fluid Dynamic theory neglected the potential energy if the height of two points in relation to a reference plane is equal. Since the height of a valve, let alone the relative height of the pilot stage, is only a few centimeters, the potential energy could be neglected. The second point within the derivation was determined by the minimum cross-sectional area of the spring element's escape passage. The first point was obtained by the definition of the initial requirement in combination of the derivation expressed in the Fluid Dynamic section. The initial requirement stated:

The escape passage of the spring element must not result in pressure drop of the pilot stage.

The derivation expressed by Bernoulli's equation and the continuity equation of fluids stated that the final pressure was determined by the relation of two points within a streamline. The requirement also specified for the pilot stage. This resulted in the first point of the derivation was obtained by the lowest cross-sectional area of the pilot stage during an uncompressed the flow. This point can be seen as "pd-restriction" in Figure 1.3. Pd-restriction consists of three holes on a component called Pilot Seat. To prevent a pressure drop within the pilot stage, the summarized area of the spring element concept's escape passages was required to be equal or greater than the summarized passage area of the pilot seat.

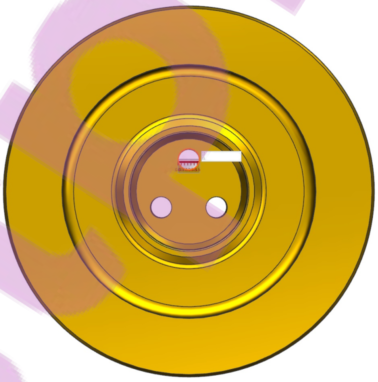

Figure 4.17.: The holes corresponds the pd-restriction

Instead of using the derivation expressed in previous chapter of fluid dynamics, the second method was performed by analyzing the current escape passage capacity. Current escape passage capacity has not created a pressure drop within the pilot stage, which is a result of an escape passage with sufficient capacity. The spring element's escape passage would meet the requirement if its capacity was equal or greater than the capacity of the current escape passage, which is the milled surface of the valve body. Calculation of the minimum cross-sectional area of the current escape passage was calculated to yield a safety factor of 4 compared to the pd-restriction.

5. Results

This chapter presents the result of concept development and the result of the final concept evaluation using finite element analysis.

5.1. Final Spring Element Concept

The final spring element concept is a cup half bulged in the shape of an ellipse, see Figure 5.1. SSAB's Form 03 was selected as the material of the spring element concept which is a high performance ductile steel recommended for deep drawing process. The concept has a positive draft and an even material thickness which are required when using deep drawing as a manufacturing process. The cutout of the upper surface can effectively be manufactured by one punch solely. The cutout enables the hydraulic flow passage. The concept is 6 mm deep and has an inner bend radius of 0.5 mm which yields a bend allowance of 1.04 mm. Insufficient material data has been provided to validate if the bend allowance is acceptable and at what degree dilutions would occur using deep drawing. By nominal dimensions, the greatest width of the concept is 22.35 mm. The concept is designed to minimize required material removal of the armature and the valve body.

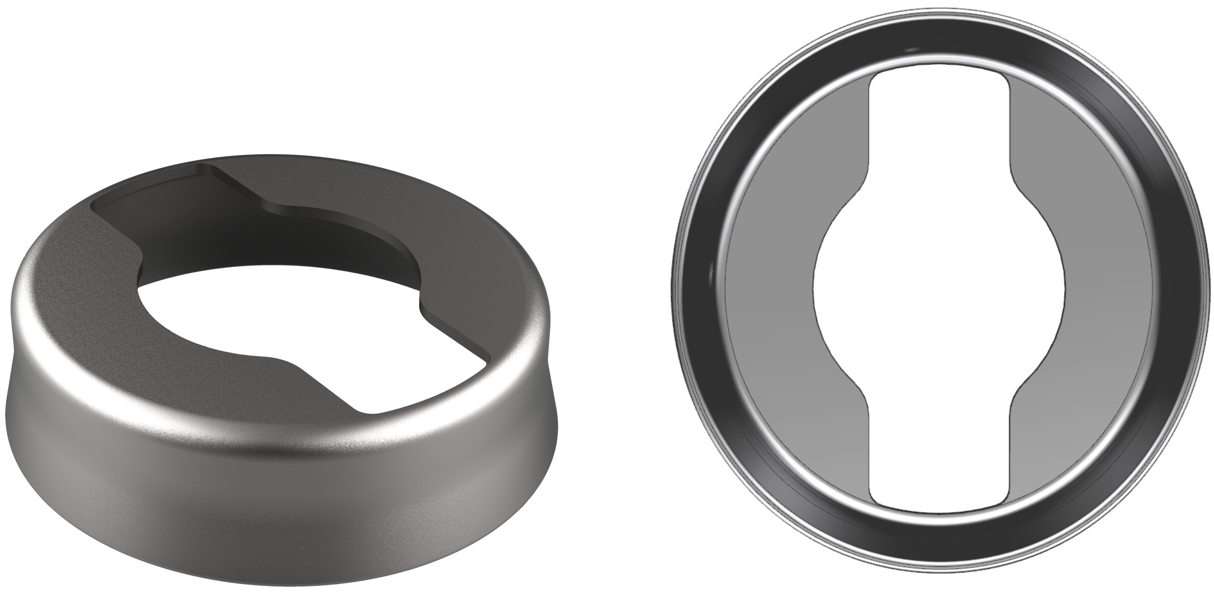

(a) Isometric view

(b) Bottom view

Figure 5.1.: Final spring element concept made of SSAB Form 03

The concept was designed to maximize the spring functionality with every other requirement taken into account. Maximum spring functionality is achieved by a maximized lever arm distance to a press fit. An ellipse shaped concept was determined to allow maximum spring functionality as its lever arm distance is solely limited by the size of the concept. An ellipse is defined by two axes, a major axis and a minor axis. The internal press fit, the interference of valve body and concept, was achieved by the minor axis of the concept was lower dimensioned than the outer diameter of the valve body. This yielded a symmetrical variable press fit but it prevented an uniform press fit, see Figure 5.2. To minimize stresses within the material and simplifying the assembly, the chamfer angle of the valve body was steeper designed and the chamfer fillet was increased. Larger fillet of the valve body and larger radius of the inside bulged radius yielded a softer assembly.

Using an ellipse shaped concept also yielded critical parameters. Displayed in Figure 5.2b, the dimensional difference of an ellipse shaped concept and a circular shaped valve body formed the escape passage. By the spring functionality of the spring element concept, the escape passage capacity would decrease as the external interference was increased. The escape passage gap was solely determined by the interference which determined the dimension and tolerance of the armature. Both enabling a hydraulic flow and allowing for a wider tolerance range were parameters which must not be compromised. The gap of the escape passage could be increased by increasing the major axis of the concept, but it would have required additional material removal of the armature's interface, which could potentially have caused the threads of the other armature surface to dislocate.

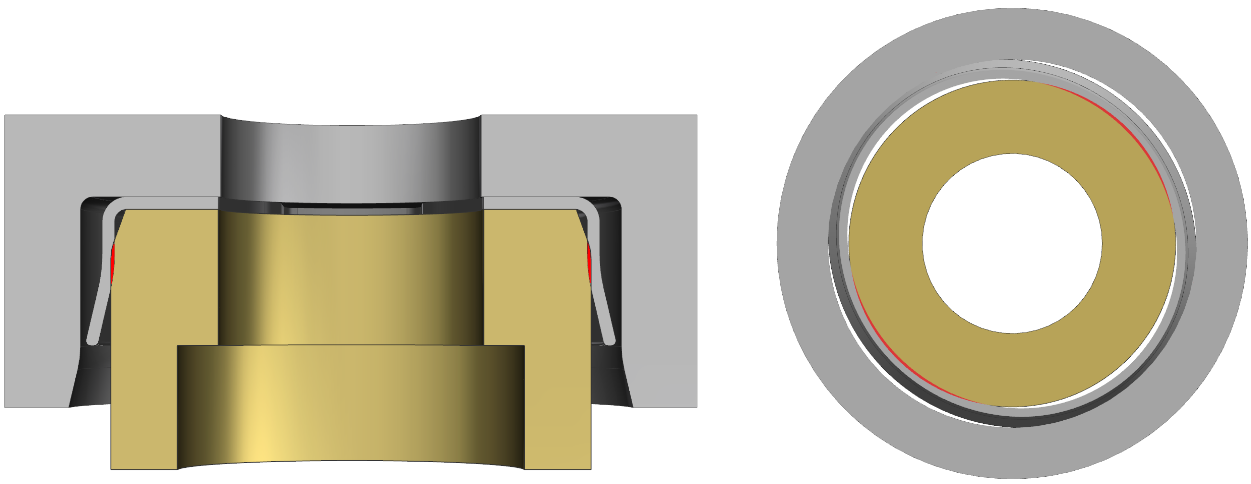

(a) Sectional side view

(b) Sectional top view

Figure 5.2.: Sectional views displaying the interferences (red) of the internal press fit

By rotating the sectional side view 45° around Z-axis and lowering the sectional top view in Z-direction of the previous figures, interferences of the external press fit can be displayed, see Figure 5.3. The spring element concept also yielded a symmetrical variable press fit but prevented an uniform external press fit. The ellipse shaped concept enabled a hydraulic flow to pass through the two dimensional differences and by the punched out surface of the concept, see Figure 5.3a. This enables a symmetrical hydraulic flow and a symmetrical press fit. This would not be possible using a circular shaped spring element without compromising spring functionality or symmetry requirements. The bulged angle was a critical parameter. A too large bulge angle would have yielded an increased disassembly force, but it would increase the required assembly force and stresses within the material significantly. It has been designed taking both parameters into consideration.

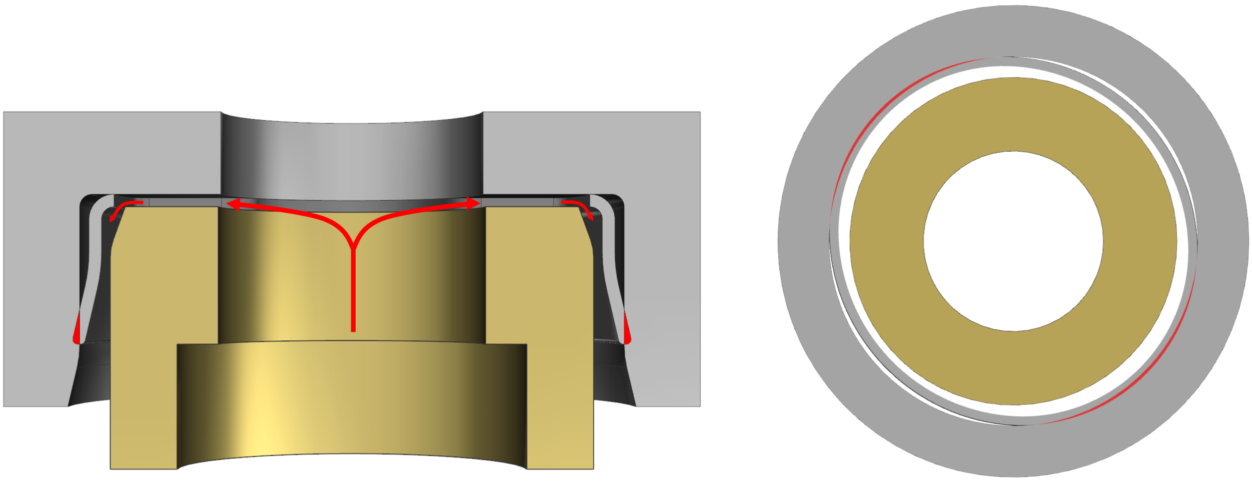

(a) Sectional side view

(b) Sectional top view

Figure 5.3.: Sectional views displaying the interferences (red) of the external press fit and the escape passage

By using the ellipse shaped spring element, the press fits were predicted to counteract, which was justified by previously mentioned nominal simulations. Counteracting press fits are a critical weakness which may result in a too low disassembly force. Simulations of a concept with no bulge resulted in fully counteracting press fits. The bulge was additionally added to potentially decrease the relation of the counteracting press fits. The bulge could potentially decrease the relation causing counteracting press fits by preventing a uniform shaped concept in Z-direction. The bulge also enables for an easy assembly as the press fit is gradually increased.

5.2. Tolerance Widths

Several interference combinations were simulated to fully utilize the grip interval. The results showed that the internal press fit was required to be nominally greater than the external press fit. This resulted in the difference of the interferences of worst case 1 was minimal.

Table 5.1 displays the nominal dimensions, tolerances and the yielded interferences which were evaluated. Tolerances of the armature and the valve body were evaluated using a tolerance width of 0.05 mm. Compared to the current tolerance widths which were 0.04 mm of the armature and 0.02 mm of the valve body. Evaluation of lower tolerance widths was determined to yield an insufficiently low economical benefit. Similar tolerance widths to the current solution were evaluated to determine if the spring element concept was feasible as early in the evaluation stage as possible.

The absolute outer diameter of the spring element refers to major axis of the ellipse located at the edge of the bulge. The absolute inner diameter of the spring element refers to the minor axis of the ellipse located at the non-bulged part of the concept.

Component	Armature	Spring Element Concept		Valve Body	Interference	
Measurement	Interface Ø	Absolute outer Ø	Absolute inner Ø	Absolute outer Ø	A - C	VB - C
Worst Case 1	21.875 + 0.025	22.35 - 0.05	19.05 - 0.05	19.325 + 0.025	0.40	0.35
Worst Case 2	21.875 - 0.025	22.35 + 0.05	19.05 + 0.05	19.325 - 0.025	0.55	0.20

Table 5.1.: Dimensions, tolerances and interferences of the worst cases displayed in mm

5.3. Worst Case 1

Maximum Stress

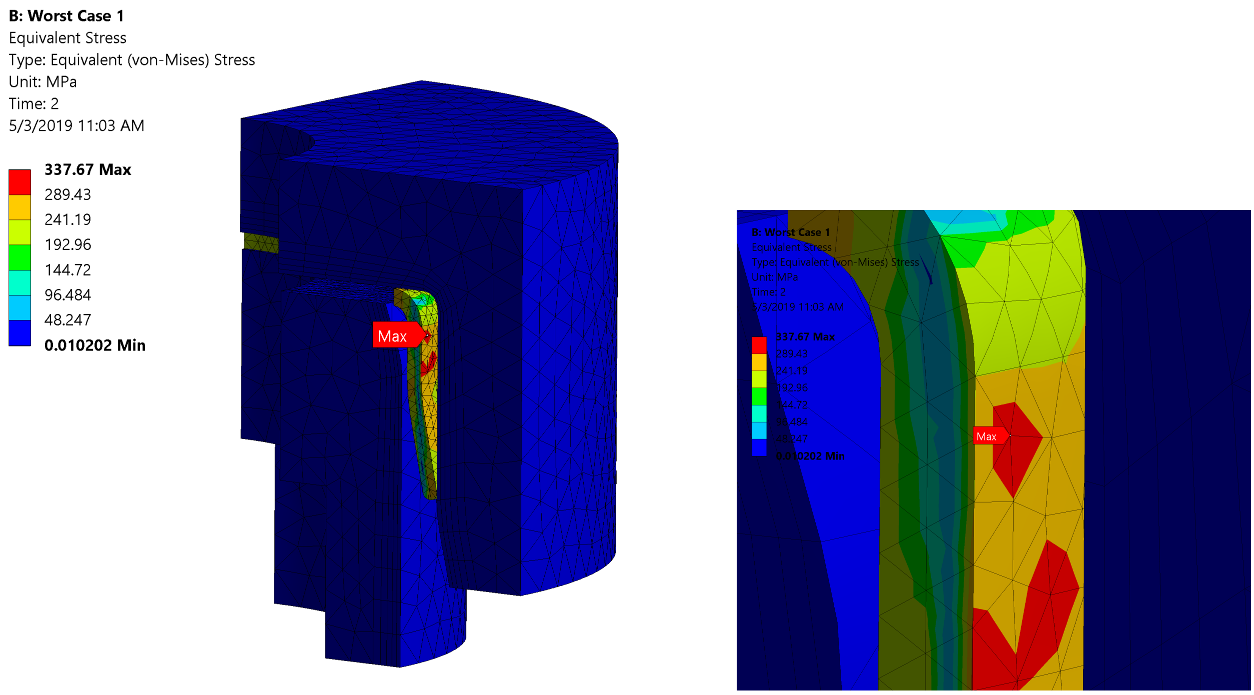

(a) Maximum stress occurred at the spring element

(b) Closer look of the outer side, major axis of the spring element which experienced the largest stress

Figure 5.4.: Maximum stress of the model occurred at load step 2 i.e, a fully assembled model

Maximum stress of worst case 1 occurred on the spring element concept at load step 2 i.e., a completed assembly of the components. The stress was computed to 337.67 MPa, which was below the true ultimate tensile strength of the spring element's material. The maximum stress was located at the major axis of the non bulged area of the concept, see Figure 5.4. The location and size of the stress may be a result of a maximum internal press fit which caused significant deformation of the major axis outer surface. The assembly of the armature may also have enforced deformation of which the spring element was pulled downwards by the motion of the armature during assembly. The valve body and the armature experienced no significant stresses as their material thickness was relatively high compared to the spring element.

Deformation

Worst case 1 was modeled to achieve the largest internal press fit. This caused the deformation of inner surface of the valve body to be the most critical. Due to this, the deformation of the inner surfaces of the valve body were solely evaluated for worst case 1.

The valve body has two critical surfaces, the upper inner surface as which the pilot seat is assembled using press fit, see Figure 5.5a and the lower inner surface which acts as a sliding contact, see Figure 5.5b. The deformation of the surfaces was evaluated using changes in nodal locations of the surfaces.

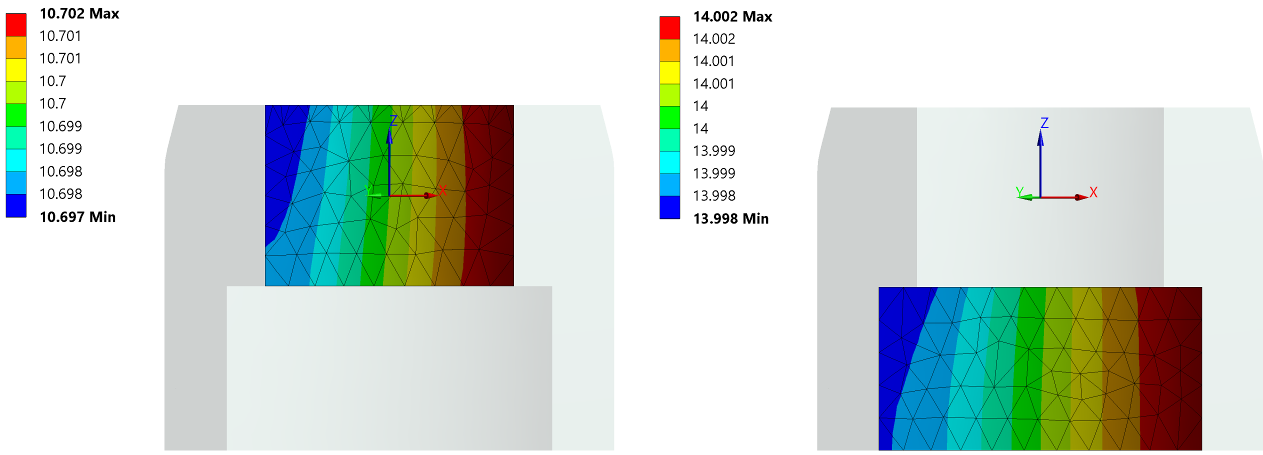

(a) The result displays a total deformation of 0.005 mm in diameter

(b) The result displays a total deformation of 0.004 mm in diameter

Figure 5.5.: Total deformation in diameter of two critical surfaces of the valve body

Causing no deformation was inevitable using a press fit assembly method. Causing no critical deformation as the requirement states refers to deformations which does not impact any functions of the valve. To determine which deformations were critical and which were not, a comparison of the resulted deformation and dimensional tolerances of the surfaces was performed. The total deformations of 0.004 mm and 0.005 mm compared to the surfaces tolerances were approved to be neglected by engineers at Öhlins Racing in Jönköping.

The upper inner surface experienced the largest deformation. A total of 0.005 mm in diameter compared to the lower which experienced 0.004 mm. The press fit of the concept and the valve body was intentionally designed to be located at the thicker area of the valve body to minimize the strain of the sliding surface.

Assembly and Disassembly Force

Assembly and disassembly forces have been evaluated using reaction forces which were generated as a component either was assembled or disassembled. Worst case 1 was modeled with the weakest external press fit and the greatest internal press fit. Therefore, the assembly force of the valve body and both assembly and disassembly force of the armature was determined to be most critical for worst case 1. The assembly of the valve body was performed at load step 1. Figure 5.6a displays a total assembly force of 71 N, which considering an automated assembly process was determined to be approved.

Disassembly force was the most critical. The disassembly force corresponds to whether the assembly can endure transportation and mounting without disassembling. Figure 5.6b displays the total required assembly and disassembly force of the armature. The maximum assembly force of the armature was computed to 10 N at the second load step. Resulting disassembly force was computed to 32 N at the fourth load step. 32 N was compared to the total weight of the valve body assembly which yields a safety factor of 105.

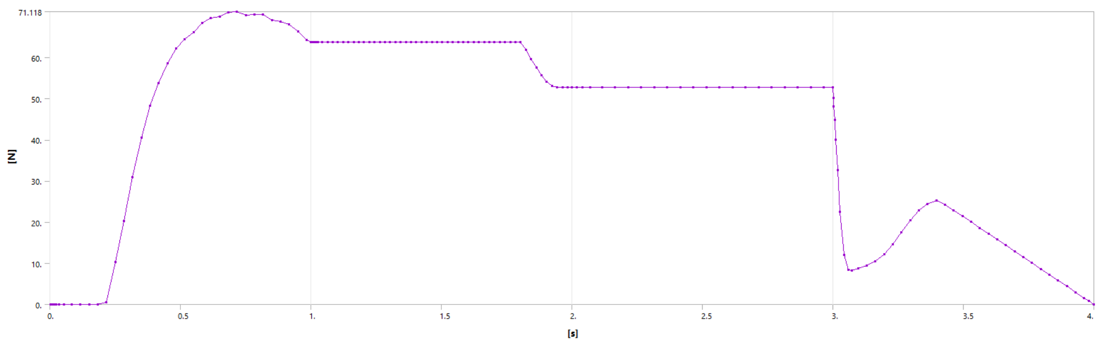

(a) Valve body assembly force 71 N at first load step

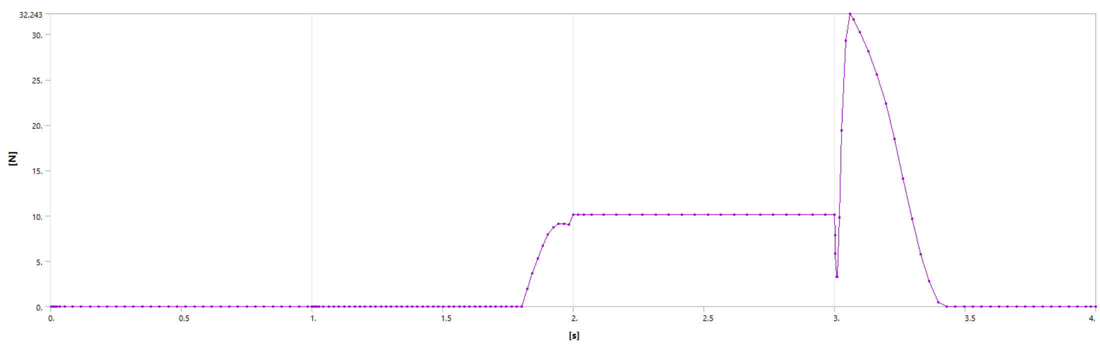

(b) Armature assembly force 10 N at second load step and disassembly force 32 N at fourth load step

Figure 5.6.: Reaction forces of the valve body (a) and the armature (b) in worst case 1

Contact Status

Contact Status in ANSYS displays the status of a defined contact. Contact status sliding is equivalent to surfaces in contact and contact status sticking is equivalent to interpenetration of surfaces. Contact status can be utilized to analyze the behavior of press fits and form relations to which disassembly force was obtained. Figure 5.7a & 5.7b displays the contact status of the internal press fit during assembly. The contact status displays minimal decreased press fit capacity as the armature was assembled. There was no sign of counteracting press fits in worst case 1.

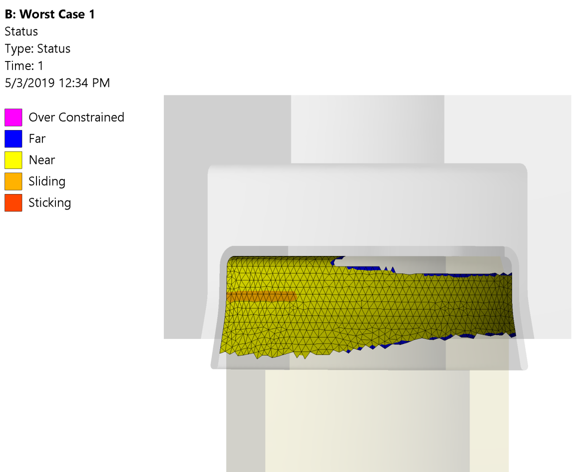

(a) Contact status at load step 1

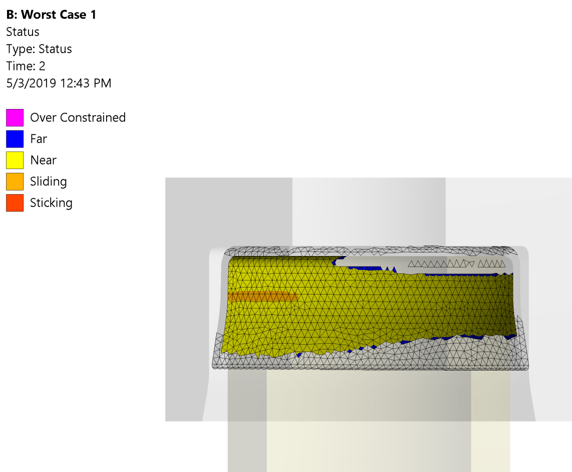

(b) Contact status at load step 2

Figure 5.7.: Contact status of the valve body and concept during the assembly

Figure 5.8 displays the contact status of the external press fit. The contact area was minimal, in a fully scaled model the summarized contact area would be of a factor 4. Regardless of the contact area, the disassembly force yielded 32 N.

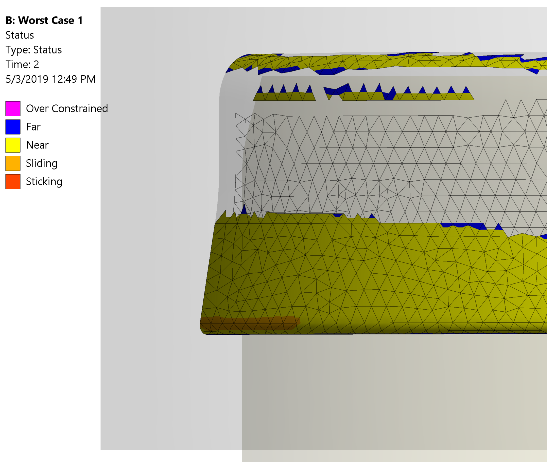

Figure 5.8.: Press fit of the armature and the concept displayed in orange

5.4. Worst Case 2

Maximum Stress

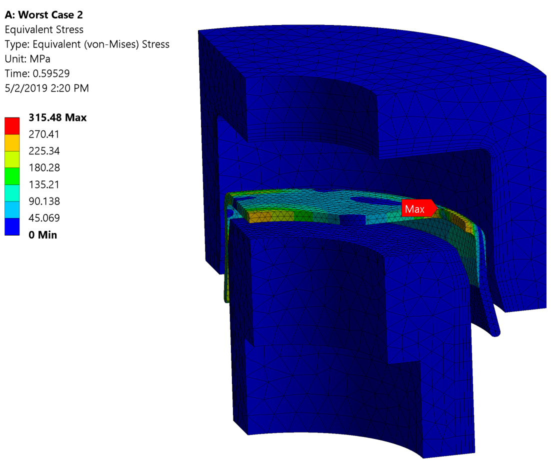

(a) Maximum stress of the model occurred at the spring element

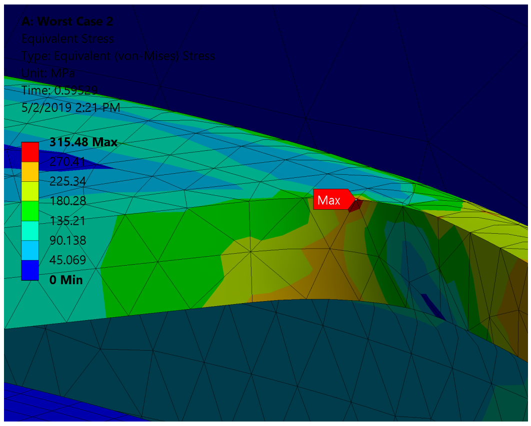

(b) Closer look of the sharp edge which caused maximum stress of the model

Figure 5.9.: Maximum stress of the model occurred at load step 0.6 i.e, the assembly of the spring element

The maximum stress of worst case 2 occurred during the assembly of the concept. Maximum stress was located at the top surface's major axis at the corner of which the concept has been punched, see Figure 5.9b. A 90° angle increases the stress concentration which could cause an exponentially increased stress of concentrated area. The maximum stress was computed to 315.5 MPa, which was lower compared to the stress computed in worst case 1. The maximum stress values and locations can't be compared due to the maximum stresses occurred at different load steps. The armature and the valve body experiences no significant stresses due to their material thickness.

Deformation

In worst case 2, the interference of the external press fit was the greatest. It was concluded that the deformation of the outer surface of the armature was the most critical in worst case 2. Similar to the performed evaluation of deformation in worst case 1, the deformation was evaluated using nodal differentiation. Figure 5.10 displays the total deformation of the armature's diameter in mm. The nominal dimension of the outer surface is 27.9 mm. This yields a total deformation width of 0.005 mm. Compared to the current tolerance of the thread, the deformation could be neglected, which was assured by engineers at Öhlins.

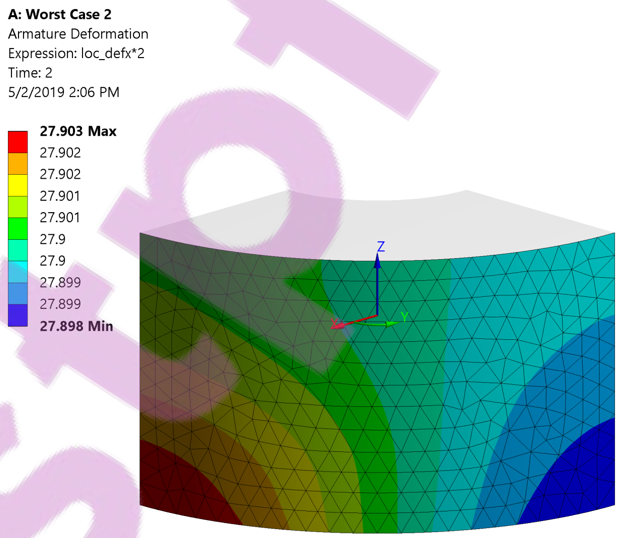

Figure 5.10.: Total deformation of the outer surface of the armature i.e, the location of the threads, displayed in changes of the diameter in mm

Assembly and Disassembly Force

Worst case 2 was modeled with the greatest interference of external press fit and the smallest of the internal press fit. This resulted in an increased assembly force of the armature and a decreased assembly force of the valve body. Assembly force of the valve body was computed to 52 N and a disassembly force 0 N. Figure 5.11a displays the assembly force at the first load step and the disassembly force at the fourth load step.

Armature assembly required a force of 72 N to be fully assembled. The reaction forces of the armature is presented in Figure 5.11b and the assembly force is obtained at the second load step.

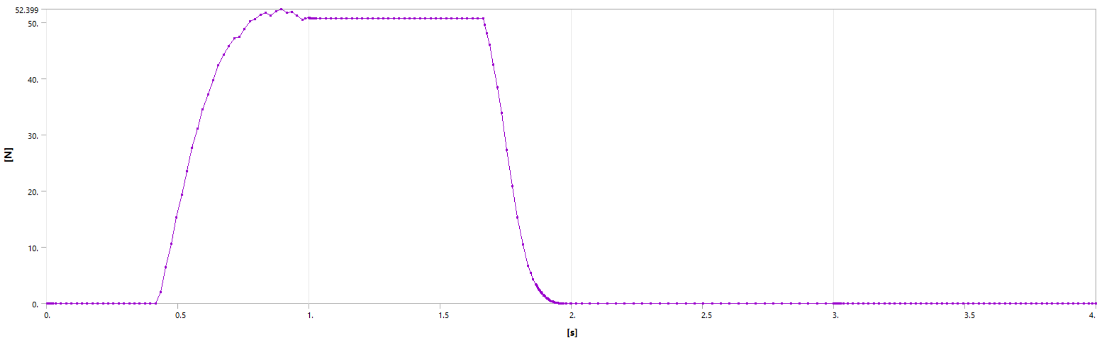

(a) Valve body assembly force 52 N at first load step and disassembly force 0 N at fourth load step

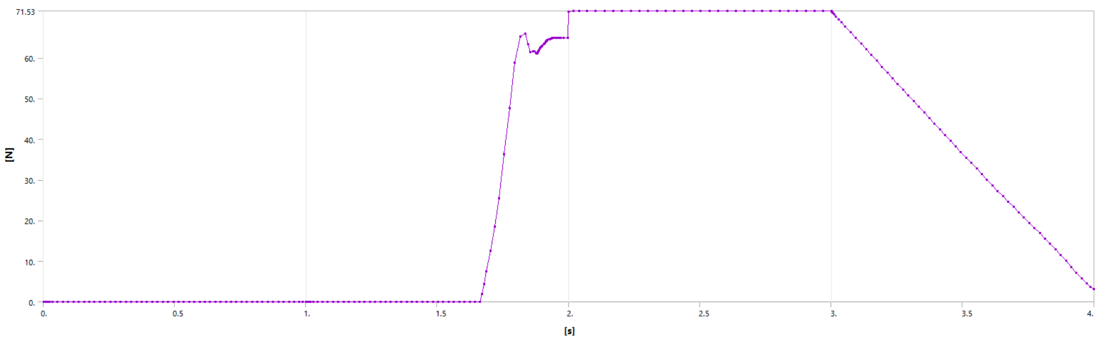

(b) Assembly force 72 N at second load step

Figure 5.11.: Reaction forces of the valve body (a) and the armature (b) in worst case 1

Contact Status

Similarly to worst case 1, the disassembly force of worst case 2 was analyzed by evaluating the contact statuses. The evaluation of contact statuses in worst case 2 was performed by analyzing the contact status of the internal press fit before and after the armature was assembled.

Figure 5.12 displays the significant decreased contact status as the armature was assembled. The significant decrease of contact status caused a decrease in the internal press fit capacity. The decreased area of contact was the decisive cause of a disassembly force result of 0 N.

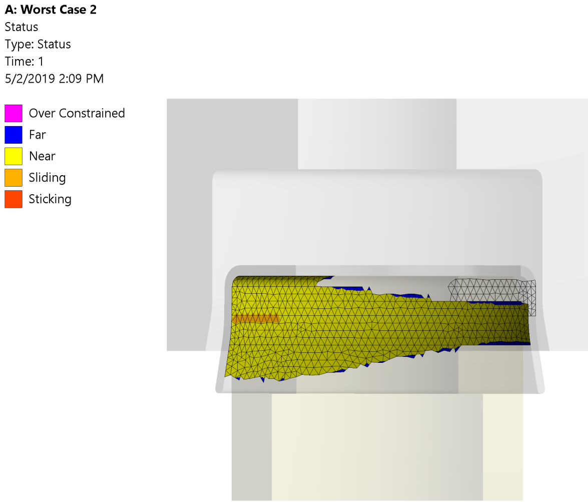

(a) Contact status at load step 1

(b) Contact status at load step 2

Figure 5.12.: Contact status of the concept and the valve body at different load steps

Compared to worst case 1, the result of worst case 2 contact status evaluation displayed an increased impact of armature assembly. The combination of one weakened interference with one increased interference was the cause of a significant decrease in contact. Figure 5.13 displays the contact status external press fit, which was increased significantly compared to worst case 1. Counteracting press fits occurred in worst case 2.

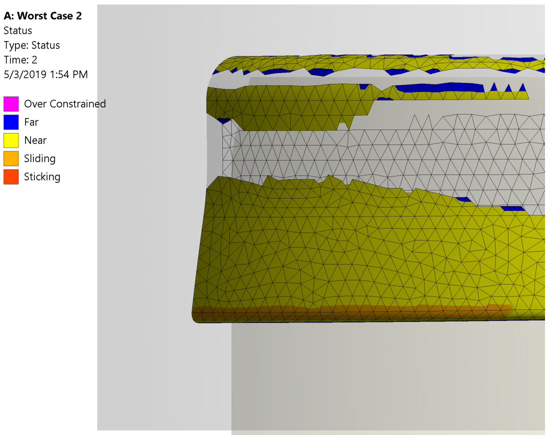

Figure 5.13.: Increased press fit capacity, displayed in orange, of the armature and the concept

5.5. Escape Passage

To achieve a reliable result if the escape passage met the requirement of no pressure drop allowed in the pilot stage, the evaluation was calculated using the lowest cross-sectional area within the escape passage. Figure 5.14 displays the location of the most critical cross-sectional area of the escape passage. The location was in Z-direction, at the same height as the press fit of the valve body and the concept but at the major axis of the ellipse. The lowest cross-sectional area occurred in worst case 1. Worst case 1 yielded the most critical escape passage as the interference of the internal press fit was the greatest. The decreased escape passage capacity was caused by the design of the concept. As the ellipse shaped concept was assembled onto the circular valve body, the shape of the spring element tried to replicate the shape of the valve body. This caused the gap between the ellipse shaped concept and the circular valve body to decrease, which decreased the escape passage.

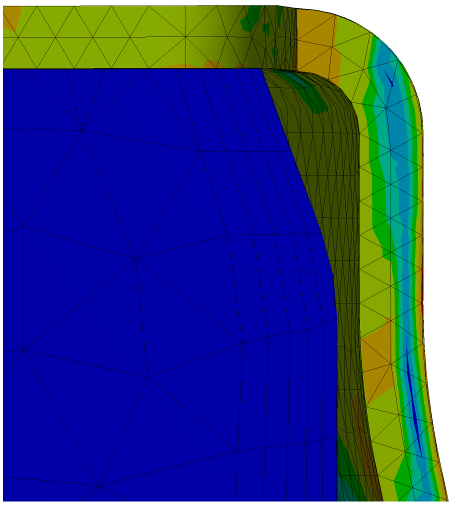

Figure 5.14.: Location of the most critical cross-sectional area within the escape passage is located at the fillet of the chamfer

Contact gap in ANSYS was utilized to provide the measurement of the gap between the valve body and the spring element concept Figure 5.15a. The gap corresponds to the height of the cross-sectional area.

Displayed in Figure 5.15b, the width of the cross-sectional area was obtained by the width of the spring element passage.

To obtain the total escape passage capacity, the width and the height were multiplied by two, since the spring element enables two symmetrical escape passages.

Total minimum escape passage capacity yielded a safety factor of 1.8 compared to the capacity of the pd-restriction. Safety factor 1.8 was achieved by evaluation of the escape passage during the least favorable extreme tolerances. Due to normal distribution of manufacturing, a safety factor of 1.8 will rarely be obtained.

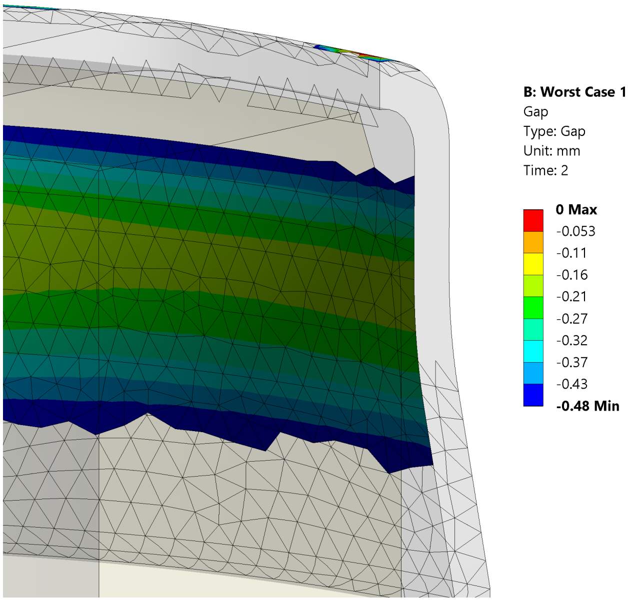

(a) Minimal gap obtained using contact gap in ANSYS

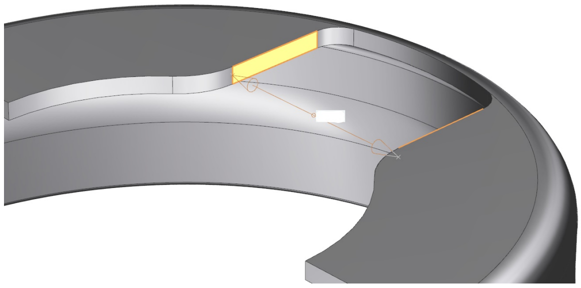

(b) Escape passage width of spring element

Figure 5.15.: The lowest cross-sectional area of the escape passage is determined by the width and the gap

6. Discussion

Discussion of implications and lessons learned regarding this problem are presented in Chapter 7.

6.1. Implications

Implications, uncertainties and suggestions of improvement are presented in this section.

6.1.1. Brainstorming and Pugh Matrix

To fully utilize concept generation, several participants are required. In this thesis, brainstorming was solely performed by the author himself. This restricts the method and the benefits of having several creative participants which combined creates concepts. Several participants bring additional viewpoints of a given problem which may result in a creative solution.

Concepts had to be eliminated to obtain a final concept. The elimination had to be performed with several requirements unanswered. Gut feeling and concept comparision of several non critical requirements determined the final concept. This may have resulted in a concept with not the best potential of meeting each requirement being evaluated using FEA.

The most optimal would have been having several participants performing concept generation and by evaluating several concepts using FEA.

6.1.2. Friction Coefficient

An essential area in this thesis was contact mechanics. To ensure a reliable result of the simulation, the friction coefficients are extremely crucial. To obtain true friction coefficients, the specific alloying materials used with corresponding surface roughness achieved by respective manufacturing methods had to be produced. These values haven't previously been produced and delivery time of desired material samples prevented an experimental evaluation to be performed. Instead, a general value of friction coefficients of the material combinations was used. These general values didn't take alloying materials in account and categorized surface roughness by dry or lubricated surfaces and not by manufacturing methods. This results in an uncertain value of friction coefficients which may affect the final result.

6.1.3. Simulated Spring Element Model

To achieve a true result of the simulation, the cad model of the spring element must be similar to a manufactured spring element. A manufactured spring element using deep drawing experiences dilution at the bend radius. The 3D model in NX was not modeled with dilutions but with an uniform material thickness. This results in a simulation result with increased solid mechanics of the spring element. If the dilution is critical, the result of the simulations may have resulted differently.

6.1.4. Computation Time

Computation time has been a critical parameter in this thesis. The computation time couldn't be decreased due to the model consisting of a 3D nonlinear contact problem which prevented simulation in 2D. Simulations requiring five hours each limits an effective work. This is partially the cause of a single concept could just be evaluated using finite element analysis.

6.2. Lessons Learned

To fully evaluate the feasibility of an additional component manufactured using a deep drawing process, the friction coefficient must be known. A simulation using worst case 1 dimensions with the upper range of friction coefficient of steel - steel contact provided a different result. Instead of the armature being disassembled, which was the main purpose of worst case 1, the valve body was disassembled. This displays the significance of friction coefficient. An increased friction coefficient may not require a large contact area to maintain assembly during e.g, transportation.

Spring functionality was a high priority when concepts were evaluated. Spring functionality did not cause any requirements not to be met. The results displayed however, that contact statuses and friction coefficient to be the cause of an unmet requirement. This may has caused an incorrect priority of achieving the greatest spring functionality instead of achieving larger contact statuses. Concepts might have been eliminated by an incorrect prioritization.

The difficulty using an additional component is achieving two different press fits of a single component, an external and an internal press fit. This entails implications of counteracting press fits, which is not desired. A suggestion of future solutions is to generate solutions which do not include an additional component. Instead, design changes of the already existing armature or valve body should be evaluated. If the interface of the armature enables spring functionality, only one press fit is required and tolerances of the valve body could potentially be increased.

7. Conclusions

This chapter summarizes if each requirement was fulfilled and which issues were answered.

7.1. Requirements Summary

It could be concluded that the solid mechanics of the spring element was approved by stresses which not exceeded the material's ultimate tensile strength. A highly prioritized requirement stated that no critical deformation of the valve body's inner surfaces and the armature's threads must occur. Deformation evaluation was performed by a comparison to the surfaces tolerances, which determined that the deformations could be neglected. The escape passage was evaluated at the least favorable dimensions but, compared to the pd-restriction, it yielded a safety factor of 1.8. Safety factor of 1.8 defines the capacity ratio of not causing a pressure drop within the pilot stage. Safety factor 1.8 was computed with the least favorable parameters, which according to the normal distribution of manufacturing rarely will be obtained.

Required assembly forces of the armature and the valve body in both worst cases were computed to a maximum of 72 N, which considering an automated assembly process is approved. The disassembly force of the valve body in worst case 1 was computed to 32 N, which compared to the mass of the valve and the gravitational force yielded a safety factor of 105. A safety factor of 105 doesn't include which g-forces the valve experiences during transportation or assembly, which prevents the disassembly force of worst case 1 to be approved without a more in depth evaluation. Worst case 2 required no disassembly force to disassemble the armature, which without a further evaluation could be determined not approved. Significant decrease in contact status of the internal press fit as the armature was assembled was the decisive cause of no disassembly force required.

7.2. Answered Issues

- How should the spring element be designed to meet the requirements?
  - Since each requirement wasn't fulfilled by the spring element implementation, the first issue of how a spring element should be designed to meet each requirement could not be answered
- How should the solid mechanics of the spring element be evaluated?
  - With a finite element analysis which with high accuracy and efficiency could provide data regarding each requirement.
- Which material is suitable for such spring element in such conditions?
  - SSAB's Form 03 which is a soft steel alloy recommended for deep drawing process. The material didn't reach fracture stresses during spring element evaluation which implies the material could sustain such conditions it experienced.

8. Future Work

- Produce or order data of precise friction coefficients with correct surface roughness and material
- Evaluate the feasibility of implementing spring functionality of the armature, which reduces the press fits to solely one

Bibliography

[1] ANSYS. *Training Manual*. Mar. 6, 2019.

[2] B. Lundkvist. *Ritteknik*. 7th ed. Liber, 1997.

[3] D. L. Logan. *A first course in the finite element method*. Fifth. Global Engineering, 2012.

[4] Carbide Depot. *Coefficient for Static Friction Steel*. Mar. 7, 2019. URL: http://www.carbidedepot.com/formulas-frictioncoefficient.htm.

[5] K. Storck, M. Karlsson, I. Andersson and D. Loyd. *Formelsamling i termo- och fluiddynamik*. 2010.

[6] N. Strömberg. *Nonlinear FEA and Design Optimization for Mechanical Engineers*. 3rd ed. 2012.

[7] Sharcnet. *Advanced Settings*. Apr. 3, 2019. URL: https://www.sharcnet.ca/Software/Ansys/17.0/en-us/help/wb_sim/ds_Contact_Advanced.html#ds_Normal_Stiffness.

[8] Sharcnet. *Solid186*. May 2, 2019. URL: https://www.sharcnet.ca/Software/Ansys/15.0.7/en-us/help/ans_elem/Hlp_E_SOLID186.html.

[9] Sharcnet. *Solid187*. May 3, 2019. URL: https://www.sharcnet.ca/Software/Ansys/17.0/en-us/help/ans_elem/Hlp_E_SOLID187.html.

[10] SSAB. *SSAB Form 03*. Mar. 5, 2019. URL: https://www.ssab.se/produkter/varumarken/ssab-form-djupdragningsstal/products/ssab-form-03.

[11] Engineering ToolBox. *Friction and Friction coefficients*. Mar. 7, 2019. URL: https://www.engineeringtoolbox.com/friction-coefficients-d_778.html.

[12] W. D Callister and D. G Rethwisch. *Materials Science and Engineering*. 8th ed. Vol. SI version. 2011.

A. Mesh Independence Study

The purpose of a mesh refinement evaluation was to achieve high reliability of the simulation by analyze the mesh influence of the results. Evaluation of mesh refinement was performed by gradually increasing the mesh refinement and analyze the stresses of the results. Mesh independence study was performed of the spring element concept, which experienced the largest deformation and stresses. A component which experiences large stresses simplifies the mesh evaluation by accelerating the stress differences of different mesh models. Stresses were extracted in the same coordinates and in the same load step of the simulation to ensure a valid evaluation. The coordinates were chosen by the location of the maximum stress of the largest mesh size. Point P defines the coordinates which is displayed in Figure A.1.

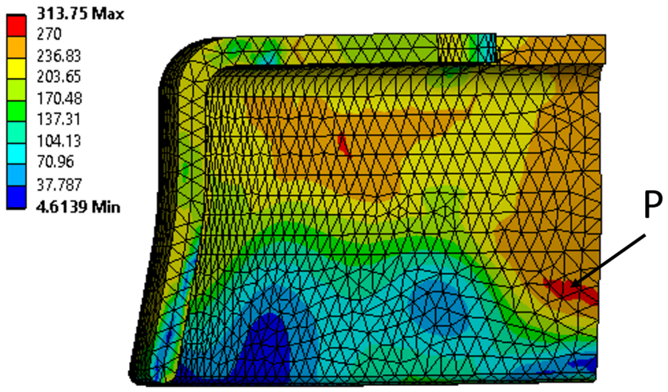

Figure A.1.: Point P displayed as which mesh independence study were performed

Six meshes with different density mesh of the spring element concept were evaluated, while the mesh of the armature and the valve body remained constant Figure A.2.

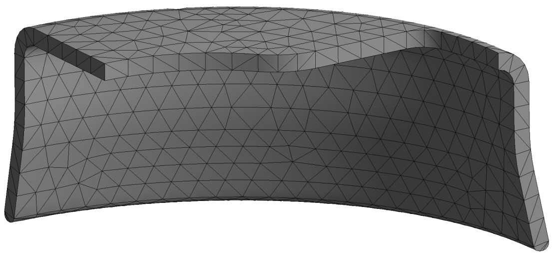

(a) Mesh sizing factor 1

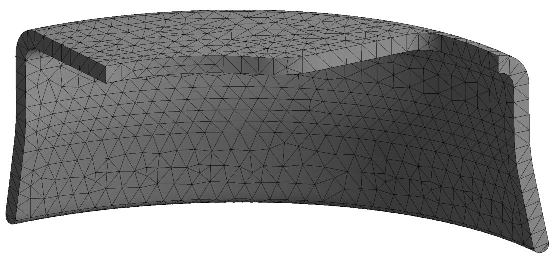

(b) Mesh sizing factor 1.5

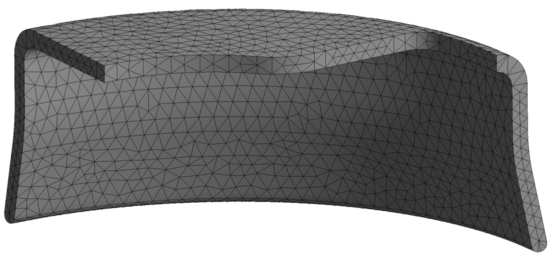

(c) Mesh sizing factor 1.8

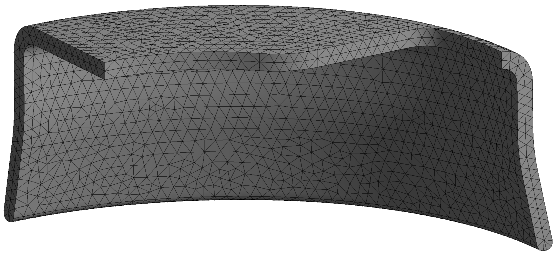

(d) Mesh sizing factor 2.3

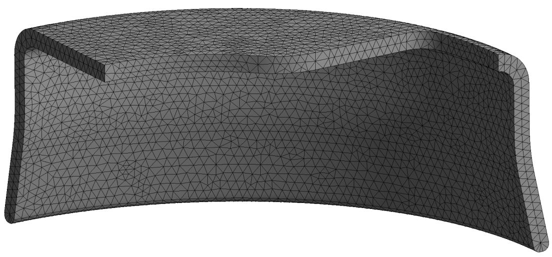

(e) Mesh sizing factor 3

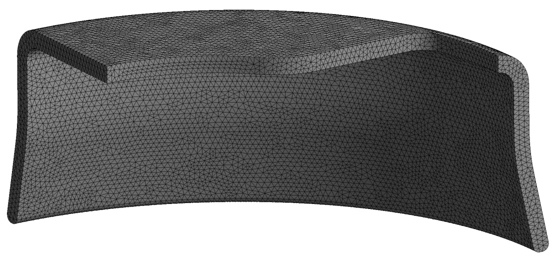

(f) Mesh sizing factor 5

Figure A.2.: The meshes which were conducted in the mesh independence study

The stress result which were extracted in point P of each mesh sizing factor can be seen in Figure A.3. It can be concluded that the mesh had great influence of the result. This is due to a finer mesh can detect stresses with more accuracy than a coarse mesh. If the extracted stresses remain constant during mesh refinement, a valid mesh has been achieved. By the result of the mesh evaluation, 3 mesh models displayed tolerably constant stress.

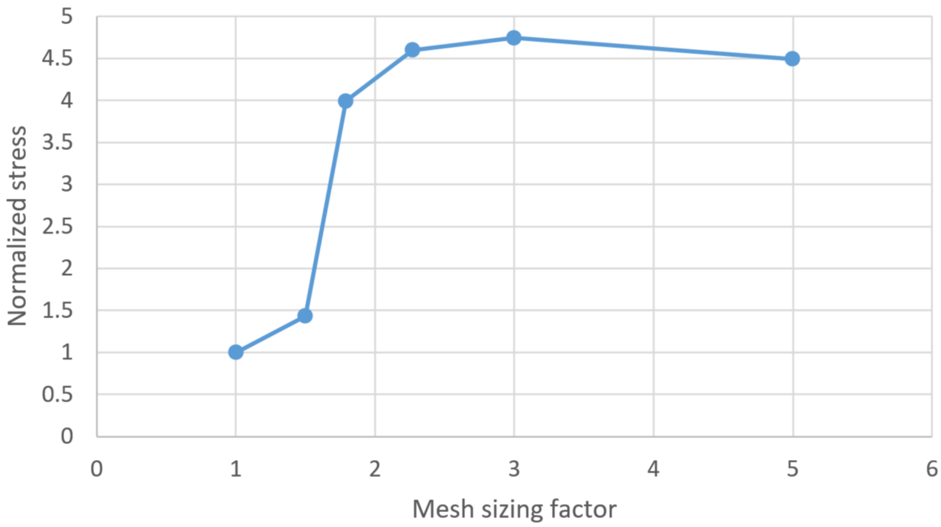

Figure A.3.: Result of mesh evaluation by gradually decreasing the element size

The 3 mesh models computation times and file storage size were then the decisive parameters of which mesh model would be used. Both computation time of the used computer and file storage were minimal, which determined a mesh sizing factor of 2.3 would be used. A mesh sizing factor of 2.3 corresponds to an element size of 0.33 mm. The element size 0.33 mm could not have been used on the entire model. To optimize the computation time of the model, non-critical components were discretized using a relatively coarse mesh which can be seen in Figure 4.14.

Elapse time and file storage size of the simulations using a mesh sizing factor of 2.3 have been summarized in Table A.1.

Worst Case	Sizing factor	Elapse time [s]	File storage size [MB]
1	2.3	9052	3247
2	2.3	18407	5938

Table A.1.: Elapse time and file storage size of worst cases using mesh sizing factor 2.3